UNIVERSITY OF BATH

University of Bath

NEW C^N^C BIS-CYCLOMETALATED Pt(II) COMPLEXES: SYNTHESIS, STRUCTURES AND PHOTOPHYSICAL PROPERTIES

Sara Fuertes, Simon K. Brayshaw, Paul R. Raithby, Stephanie Schiffers and Mark R. Warren.*

Department of Chemistry, University of Bath, Bath, BA2 7AY (United Kingdom).
Fax: (+44) 1225 383183.
E-mail: p.r.raithby@bath.ac.uk

RECEIVED DATE (to be automatically inserted after your manuscript is accepted if required according to the journal that you are submitting your paper to)

Abstract

The reaction of a new ligand, ethyl 2,6-diphenylisonicotinate (EtO_2C-C^N^C-H_2), with K_2PtCl_4 in acetic acid affords the mono-cyclometalated complex, $[\{(EtO_2C$-C^N^C-H)Pt(\mu$-Cl)$\}_2]$ (**1**), which transforms to the bis-cyclometalated derivative, $[Pt(EtO_2C$-C^N^C)(DMSO)]$ (**2**), when heated in hot DMSO. Complex **2** is the precursor for preparing a new series of neutral mononuclear bis-cyclometalated complexes $[Pt(EtO_2C$-C^N^C)(L)]$ [L= tht (**3**), PPh_3 (**4**), CN-^{t}Bu (**5**), py (**6**), py-^{t}Bu (**7**), py-NH_2 (**8**), py-CN (**9**) and py-$CONH_2$ (**10**)]. These new complexes have been characterised spectroscopically and structures of **2**-**10** have been determined crystallographically. Within each crystal structure the individual molecules pack in a head to tail arrangement. Non-covalent interactions including $\pi\cdots\pi$, C-H$\cdots$O, C-H$\cdots$N, N-H$\cdots$Pt, N-H$\cdots\pi$, C-H$\cdots\pi$ and N-H$\ldots$O contribute significantly to the supramolecular structures displayed by these complexes in the solid state. All complexes display UV-Vis absorptions in dichloromethane solution. Excitation and emission studies as well as lifetime measurements are described and can be correlated to the solid state structures of

the complexes. DFT and TDDFT computational studies have been performed on **5** and **8** which support the conclusions drawn from the photophysical studies.

Introduction

Luminescent platinum (II) complexes are attracting much attention because of their extensive photochemical and photophysical properties.[1-3] Amongst all the numerous applications in the area of material science, the platinum (II) complexes are especially appealing because of their potential use in the development of new tuneable optoelectronic molecular devices,[4-9] dye-sensitized solar cells[10, 11], as well as in sensor manufacturing[12-14] and as imaging agents for biomolecules.[15-21]

Within this field, square planar platinum (II) complexes containing aromatic molecules with delocalized π electron density such as diimines,[22-32] terpyridines,[32-40] or the cyclometalated[8-9, 13, 41-65] derivatives are suitable systems for these purposes because of the nature of their emissive states. Cyclometalated ligands display an additional advantage over purely N-donor ligands. The splitting of the *d* orbitals can be enhanced due to the strong ligand field induced by the C-σ bond. Consequently, the energy of the metal centred (MC) (d-d) excited states are raised, preventing nonradiative decay processes from occurring.[66] Cyclometalated platinum (II) complexes with a tridentate chelating ligand (C^N^N, N^C^N, C^N^S) have been extensively investigated recently.[8, 9, 52-64] However, examples of bis-cyclometalated Pt(II) complexes, resulting from a double C-H activation of the tridentate C^N^C ligand, are still relatively scarce in the literature despite having the advantage over the other "pincer" complexes of generating neutral systems, when the fourth ligand, L, is also neutral, and thus generating materials that do not require the presence of counterions. Since the first complexes [(C^N^C)PtL] (L= py, Et$_2$S, pyr) were described by von Zelewski *et al.* in 1988,[67] only a few compounds have been reported.[13, 46-51]

The platinum metal centre, being a heavy transition metal ion, can induce strong spin-orbit coupling (SOC) facilitating intersystem crossing (ISC) and, therefore, the subsequent radiative decay, both of which are spin forbidden singlet-triplet transitions.[66] A further benefit of the presence of a third row transition metal is the increased ligand-field stabilization energy (LFSE), consequently, the MC (d-d) excited states become thermally less accessible than the metal-to-ligand or intraligand charge transfer states.[1] Thus, the nature of their emissive states generally depends upon the metal-to-ligand (MLCT), or intraligand charge-transfers (ILCT), which are strongly influenced by the

properties of the ancillary ligands. Besides, as these complexes are essentially planar they can interact with each other through $\pi\cdots\pi$ or Pt$\cdots$Pt interactions creating excimers or aggregates with a consequent change in the nature of the emissive state ($\pi\pi^*$ or MMLCT).[36, 43, 44, 49-51, 54, 56, 68] These transitions, $\pi\pi^*$ and MMLCT, are especially sensitive to the local environment, such as temperature, concentration, solvation and the nature of the counterion.[13, 23, 25, 31, 33, 35-36, 38, 40, 43, 44, 54, 69]

These weak interactions ($\pi\cdots\pi$ or Pt$\cdots$Pt), not only can give rise to rich photoluminescence displayed by the compounds in solid state or solution, they have also been shown to play an important role in molecular recognition, crystal engineering, self assembly and molecular electronics.[70-72] Among all the non-covalent interactions, hydrogen bonding is one of the most important driving forces in supramolecular aggregation. During the last three decades, research has shown the major importance of hydrogen bonding in many key chemical and biochemical processes.[73-76] Its strength and directionality are the main assets in the control of the supramolecular synthesis. Non-covalent interactions contribute significantly to the arrangement of smaller molecules into more elaborate structures generating a diverse number of architectures.[72, 77-80] However, structure design also strongly depends upon the coordination sites of the metal center and its electronic properties.[81-82]

Taking into account all these premises, our research work has focused on the study of luminescent complexes of Pt(II) using a new derivative of the 2,6-diphenylpyridine. Ethyl 2,6-diphenylisonicotinate (EtO$_2$C-C^N^C-H$_2$) combines both elements described above, the extended π- electron density and a functional group. The former would supply additional optoelectronic features to the platinum system whereas the latter may provide possibilities of self-assembly and also supports molecular aggregation. This promising ligand will enable us to explore the photophysical properties of new luminescent Pt(II) complexes as well as to study the correlation between optical properties and structures in solid state.

We now describe the preparation of the new 2,6-diphenylisonicotinic derivative, its mono- and bis-cycloplatination as well as the synthesis, characterization, absorption and emissive properties of these neutral bis-cyclometalated complexes [(EtO$_2$C-C^N^C)Pt(L)] [L = dimethylsulfoxide (DMSO; **2**), tetrahydrothiophene (tht; **3**),

triphenylphosphine (PPh$_3$; **4**), *tert*-butyl isocyanide (CN-^{t}Bu; **5**), pyridine (py; **6**), 4-*tert*-butylpyridine (py-^{t}Bu; **7**), 4-aminopyridine (py-NH$_2$; **8**), 4-cyanopyridine (py-CN; **9**) and isonicotinamide (py-CONH$_2$; **10**)] in which the ancillary ligands (L), with their different electron-donating or -withdrawing properties, allow for the fine tuning of the electronic properties of the "Pt(EtO$_2$C-C^N^C)" unit. The solid state structures of **3-10** have also been determined by X-ray diffraction studies. To complete the study of the "Pt(EtO$_2$C-C^N^C)" system, DFT and TDDFT computational studies have been performed on complexes **5** and **8**.

Results and Discussion

Synthesis and characterization

The synthesis of EtO$_2$C-C^N^C-H$_2$ (**A**) was achieved by a Fischer-Speier esterification of 2,6-diphenylisonicotinic acid (see Scheme 1). The reaction proceeded to completion from the analysis of the IR, NMR spectroscopic data and from C, H and N analysis (see Experimental Section for details). Subsequent cycloplatinations of this ligand were carried out following a slightly modified version of the Rourke's[46-47] method to afford the monocyclometalated complex **1** and the biscyclometalated complex **2**. Both compounds were isolated as pure solids and fully characterized (see Scheme 1 and Experimental Section) as they are air stable and soluble in common organic solvents.

<Scheme 1>

An analysis of the IR spectra of **1** and **2** shows that the ν(CO) absorptions (1726 cm^{-1} (**1**), 1716 cm^{-1} (**2**)) are similar to those in the free ligand (1715 cm^{-1} (**A**)), indicating that the ester group remains intact. The presence of the binuclear species for **1** was confirmed by ESI (+) mass spectrum (1029 [{(EtO$_2$C-C^N^C-H)Pt(μ-Cl)}$_2$ - Cl]$^+$). Well resolved ^{1}H and ^{13}C{^{1}H} NMR spectra were observed for **1** and **2**, and signal assignments were based on ^{1}H-^{1}H and ^{1}H-^{13}C correlations (see supporting information for further details).

Complex **2** was used as starting material to prepare a series of neutral complexes using different S-, C-, N- and P- donor ligands (Scheme 1). Solutions of **2** were treated with tht, PPh$_3$, CN-^{t}Bu and py to afford the corresponding complexes (**3** – **6**) in good yields.

In addition, reactions between **2** and different *para*-subsitituted pyridines have been performed. These substituted pyridine rings provide a variety of electron-donating (-*t*Bu (**7**), -NH$_2$ (**8**)) and -withdrawing substituents (-CN (**9**), -CONH$_2$ (**10**)) which may be used to establish a correlation between the electronic and spectroscopic properties. All of these complexes were obtained as pure and air stable orange solids (Experimental Section). They were characterized by elemental analysis, IR, mass spectroscopy and ^{1}H, ^{31}P{^{1}H} and ^{13}C{^{1}H} NMR spectroscopies and mass spectrometry (see supporting information). All data collected from these experimental techniques are consistent with the structures proposed for them (Scheme 1) and these structures were unambiguously confirmed by single crystal X-ray diffraction studies. The IR spectrum of **5** shows one absorption at 2163 cm^{-1} due to the ν(C≡N-^{t}Bu) which appears at similar frequencies to those observed in related complexes with terminal isocyanides[44-45, 49, 54] and, as expected, is shifted to higher energies with respect to the corresponding free ligand (2125 cm^{-1}). The ^{31}P{^{1}H} NMR spectrum of **4** shows one sharp signal with ^{195}Pt satellites. The P-Pt coupling constant is 4096 Hz comparable to those found in related complexes [Pt(C^N^N)(PPh$_3$)]ClO$_4$,[52] [Pt(C^N^C)(PPh$_3$)][49] and [Pt(Ph-C^N^C)(PPh$_3$)].[50] Signal assignments in the ^{1}H and ^{13}C{^{1}H} NMR spectra were supported by ^{1}H-^{1}H COSY and ^{1}H-^{13}C HSQC and HMBC experiments. The only remarkable feature in the NMR spectra is that C$_1$-Pt coupling constants in **4** ($^1J_{C-Pt}$ = 691 Hz) and **5** ($^1J_{C-Pt}$ = 665 Hz) are rather smaller when compared to the observed in **2** ($^1J_{C-Pt}$ = 713 Hz), whereas an increase of ∼ 20 Hz is observed in those for complexes **6-10**. This is consistent with the better π-acceptor properties of the PPh$_3$ and CN-^{t}Bu ligands compared to the pyridine derivatives.

Crystal structure determination

Single crystal X-ray diffraction studies were performed to determine the solid-state structures of the complexes. Crystallographic data for **2-10** are given in Table 1 and 2. Molecular and crystal packaging diagrams of the representative complexes **2**, **7**, **8** and **10** are shown in Figures 1-4. Selected bond lengths and angles for complex **2** are shown in Table 3. Information on the remainder of the complexes is included in the Supporting Information (Figures S1-S8 and Table S1). Complexes **2-10** show very similar coordination geometries around the metal center, therefore, we use complex **2** as a representative example of the series. The platinum (II) ion adopts a distorted square–

planar geometry with bond parameters similar to those observed in typical C^N^C tridentate platinum (II) complexes.[13, 46-50] Not surprisingly, the angle between the *trans* aryl carbon atoms (C(11)-Pt(1)-C(21) = 160.54(10)°) deviates from linearity because of the orientation of the donor atoms imposed by the R-C^N^C ligand. An additional feature of the tridentate ligand is that their Pt-C bonds (2.088(3) Å and 2.062(2) Å) are slightly elongated because of the *trans*-effect that the carbon atoms impose on each other. The dimethylsulfoxide molecule, S-coordinated to the platinum center, shows a Pt-S (2.1911(6) Å) distance similar to those reported for [Pt(R-C^N^C)(DMSO)][46-47, 49-50] The molecule is essentially flat. The sulfoxide group is almost coplanar with the Pt(C^N^C) moiety (dihedral angle 0.98° between the plane defined by Pt(1)-C(11)-N(1)-C(21) and the plane defined by Pt(1)-S(1)-O(3)). The carboxylate group also lies in the molecular plane (dihedral angle 1.08° between the plane defined by Pt-C(11)-N(1)-C(21)-S(1) and the one defined by O(1)-C(9)-O(2)), however, there is little apparent conjugation between the carboxylate group and the aromatic ring system because the C(4)-C(7) bond distance (1.491(4) Å) lies in the range for single Csp^2-Csp^2 single bonds.

In complexes **3-5**, instead of dimethylsulfoxide, a molecule of tetrahydrothiophene, triphenylphosphine or *tert*-butyl isocyanide completes the platinum coordination sphere, respectively (see supporting information). The Pt-S, Pt-P and Pt-C distances are similar to those found for related complexes.[49, 50, 52, 54, 83] The C(21)-Pt-C(11) angle in **4** is significantly smaller (158.62(6)°) than that in the other complexes (161.1(6)-162.5(8)°), because of the steric effects of the bulky phosphine ligand.

In complexes **6-10** (Figures 2-4 and supporting information), Pt-N(2) (py) (2.019-2.033 Å) distances are comparable to those reported for related structures [Pt(C^N^N)(py)](PF_6),[15] [Pt(C^N^N)(py-NH_2)](ClO_4),[84] [Pt(C^N^C)(*t*Bupy)][49] and [Pt(C^N^C)(pyCOA15C5)] (A15C5 = aza[15]crown-5)[13] and they are independent of the electron nature of the *para*-substituent. The pyridine rings are not coplanar with the Pt(C^N^C) moiety, showing dihedral angles of 57.9°(**6**), 74.9°(**7**), 66.1°(**8**), 46.9°(**9**), and 70.8°(**10**). All these values are similar to those observed in the literature.[13, 49] Complexes **6-10** exhibit Pt-N and Pt-C (C^N^C) distances which are slightly shorter when compare to those observed in complexes **2-5**. This is also related to the C_1-Pt

coupling constants obtained in the ^{13}C NMR spectra. Because the pyridine derivatives appear to be poorer π-acceptors, the bonding within the Pt-CNC moiety is stronger, showing shorter bond distances and bigger coupling constants.

Inspection of the packing within the crystals of **2-10** revealed the presence of weak intermolecular interactions including π···π,[48-50, 85] C-H···π,[48, 50, 85-88] C-H···O,[48, 50, 89-91] C-H···N,[48, 90, 92, 93] N-H···Pt,[94-98] N-H···π,[99-101] and as well as conventional N-H···O hydrogen bonding in **10**,[76, 81, 90] (Figures 1-4 and S1-S8). The combination of these weak interactions results in the packing of the monomers molecules into 2D or 3D networks. However, none of the crystal structures showed Pt-Pt interactions.

In the crystal structure of **2**, molecules stack in columns in a head to tail fashion, along the *a*-axis, with the assistance of weak π···π and C-H···O intermolecular interactions. As shown in Figure 1b, the molecules from alternate layers are totally eclipsed. Short π···π contacts in the range 3.41 - 3.74 Å are observed between the CNC ligands of neighboring molecules. There is also a weak, but we believe significant, interaction between oxygen atom O1 of the ester group and the methyl hydrogen atoms of the DMSO belonging to monomers in both adjacent layers (d (H---O) = 2.32, 2.34 Å; d (C---O) = 3.21, 3.23 Å). Along the *c*-axis, additional interactions with the monomers which belong to the same layer are creating a 2D network (Figure 1c). The oxygen atom O3 of the coordinated DMSO exhibits interactions with the hydrogen atoms of both methyl groups from an adjacent DMSO molecule located in the same layer (d (H---O) = 2.45, 2.47 Å; d (C---O) = 3.34, 3.32 Å).

The weakness of most of these C-H···O interactions is reflected by the long distance (d (C---O) = 3.21 - 3.34 Å) which is longer than conventional hydrogen bond distances, but consistent with a weakly bonding interaction between an electronegative oxygen atom center and a hydrogen on a sp[3] hybridized carbon atom.[89, 90] It is, however, strong enough to facilitate the arrangement of the monomers into a *3D* network which is very different from the packing arrangement observed in the related complexes [Pt(R-C^N^C)(DMSO)].[46, 47, 49, 50]

Likewise, neighboring molecules in complexes **3**-**10** (except **4** and **9**) are stacked in pairs in a head-to-tail fashion giving rise to different 2D or 3D networks (Figures 2-4 and S1-S8). In **4**, they show an offset π-π overlap between the aromatic rings of the tridentate CNC ligand whilst in **9**, they display a π-π interaction between the cyanopyridine and the aromatic rings of the CNC ligand. Most of the head-to-tail pairs are only supported by the π-π stacking, although complexes **4**, **7**, **8** and **10** display an additional C-H⋯O interaction between the molecular pairs. All these molecular pairs generate supramolecular structures, supported by non-covalent interactions (π⋯π, C-H⋯π, C-H⋯O, C-H⋯N, N-H⋯Pt, N-H⋯π, N-H⋯O), however no Pt-Pt contacts were observed in any of them. All the crystal structures show CH-O interactions either in the "internal" array of the molecular pairs or in the "external" array except for **5**. This weak interaction makes a considerable difference in the arrangement of the monomers, particularly when the X-ray structures of [Pt(C^N^C)(*t*Bupy)][49] and **7** are compared. They are very similar compounds but the former does not have the ester group at the back of the tridentate ligand, therefore the monomers only assemble themselves into head to tail pairs with the assistance of π-π interaction, whereas complex **7** exhibits two different C-H⋯O interactions as can be seen in Figures 2a and 2b. The first occurs between the ester and the *t*Bupy hydrogen atoms from the monomers of the same molecular pairs (Figure 2a; C⋯O 3.38 Å, H⋯O 2.53 Å). The second is between the ester and the CNC hydrogen atoms of monomers from the same layer (Figure 2b; C⋯O 3.45, 3.46 Å, H⋯O 2.51, 2.54 Å). These C-H⋯O contacts and the rest of non-covalent interactions observed in the crystal structure (π⋯π, C-H⋯N, C-H⋯π) gave rise to the supramolecular 2D network shown in Figure 2c.

As mentioned above, the crystal structure of complex **8** shows head to tail molecular pairs (Figure 3b) with rather short π⋯π (3.37-3.50 Å) and C-H (py)⋯O (ester) contacts (C⋯O 3.46 Å, H⋯O 2.51 Å). These molecular pairs are associated with the neighboring pairs through non-covalent interactions creating a 2D network. In addition, in this case, different types of weak interactions (N-H ⋯O, N-H⋯Pt, N-H⋯aromatic) are also present. The NH_2 group of the aminopyridine exhibits four different contacts (black dashed line in Figure 3c): 1) ester (N-H⋯O, N⋯O 3.13(3) Å, H⋯O 2.44(2) Å, N-H⋯O 143.95(3)°); 2) hydrogen atoms of the CNC ligand (C-H (CNC)⋯N (NH_2-py) (C⋯N 3.64 Å, H⋯N 2.69 Å); 3) carbons of the CNC ligand (N-H⋯aromatic, N⋯C

3.58 Å, H···C 2.79 Å) and 4) platinum center (N-H···Pt, N···Pt 3.56(3) Å, H···Pt 2.77(2) Å, N-H···Pt 157.08(2)°). The N-H···Pt contact parameters are slightly longer than those reported in the literature.[84, 94-97] Most of the Pt-H interactions reported so far are intramolecular,[94, 96-98] although there are a few examples of intermolecular contacts such as that found in [NPr$_4$][PtCl$_4$][cis-PtCl$_2$(NH$_2$Me)$_2$].[95] However, the ^{1}H NMR spectrum in acetone-d^6 at 203 K leaves some ambiguity as to the presence of such an interaction. The resonance corresponding to the NH$_2$ hydrogen atoms appears as a singlet at 7.00 ppm without any platinum satellites. A downfield chemical shift of the proton resonances from the free ligand value at 203 K (6.15 ppm) is observed. This downfield shift of ~ 1 ppm has been considered as a signature for N-H···Pt hydrogen bonding.[95, 97]

Additionally, in the structure of **8** (Figure 3c) we find an edge-to-face π interaction, one of the aminopyridine hydrogen atoms (H$_m$, the hydrogen in the *meta* position) is pointing to the center of the phenyl ring of the CNC ligand, showing rather short distances: C-H···aromatic (C···*Cg* 3.62 Å, H···*Cg* 2.41 Å, C-H···*Cg* 173.7°; *Cg* is the centroid of the phenyl ring).[86-88] However, the ^{1}H NMR room temperature spectrum does not show the H$_m$ signal shifted upfield as it would be expected due to the π shielding,[86, 102-103] therefore, this weak interaction is no longer retained in solution. The combination of these intermolecular interactions results in a supramolecular network with channels which are occupied by dichloromethane molecules.

The X-ray structure of the isonicotinamide derivative (**10**) displays a strong hydrogen bonded component. Perspective and crystal packaging drawings of **10** are shown in Figure 4. The molecules are stack into pairs in a head to tail fashion with the assistance of π···π and C-H···O interactions (π···π 3.31 Å C···O 3.33 Å, H···O 2.66 Å) (Figure 4b). As is shown, these molecules also show two different hydrogen bonds with the neighboring molecules. The first hydrogen bond is found between the amide groups of monomers belonging to the same layer (N···O 2.908(2) Å, H···O 2.15(2) Å, N-H···O 166.7(3)°). The second hydrogen bond interaction occurs between the amide group and the ester from monomers belonging to adjacent layers (N···O 3.062(3) Å, H···O 2.28(2) Å, N-H···O 172.9(3)°). This second interaction presents more elongated bond distances when compare with the first one and both lie in the upper range of those observed for

hydrogen bonds.[76, 81, 104-106] Despite the weakness of these interactions, which is reflected in the long contact parameters (d (N---O) = 2.90 - 3.06 Å), they are strong enough to arrange the monomers into a 3D network.

Absorption spectroscopy and theoretical calculations

UV-Visible spectroscopy was performed on complexes **2-10**, and UV-Vis spectral data are listed in Table 4. All complexes display structured bands at 350-375 nm ($\varepsilon > 10^4$ M^{-1} cm^{-1}) with vibronic differences (ca. 1300 cm^{-1}) in agreement with the skeletal frequency of the ligand C^N^C (see Figure 5). These absorptions appear to be fairly insensitive to the ancillary ligand and show a slight solvatochromic effect (2 nm shifts) in acetonitrile solutions. Complexes **3** and **6-10** show a modest shoulder at around 400 nm ($\varepsilon \approx 3 \cdot 10^3$ M^{-1} cm^{-1}) which seems to be slightly red-shifted (410 nm) in the amino derivative (**8**). Additionally, the UV-Vis spectra of all complexes show weaker bands at lower energies 470-550 nm ($\varepsilon \approx 0.2 \times 10^3$ M^{-1} cm^{-1}). To determine whether these bands were associated with intermolecular transitions, we acquired absorption spectra of **8** at concentrations ranging from 10^{-3} to 10^{-6} M. As shown in Figure S10, the absorptions at 410, 515 and 552 nm obey Beer's Law, suggesting that no significant aggregation occurs within this concentration range. On the basis of literature results,[13, 48-50] the 350-375 nm bands are assigned to metal-perturbed ligand centered transitions (^{1}LC $\pi \rightarrow \pi^*$) of the R-C^N^C ligand, whereas those at ~ 400 nm are attributed to ^{1}MLCT (5d(Pt)$\rightarrow\pi^*$(CNC)).[49, 84] Solvatochromic effects in either MeCN or MeOH solutions of **8** (see Figure S11) support this assignment as well as the comparison of the electronic absorption spectra depicted in Figure S12. As shown in the latter one, the 400 nm band appears slightly red shifted for complexes **7** and **8**, which are the pyridine derivatives *para*-substituted with an electron donating group. Finally, the lower energetic bands (515 and 552 nm) are assigned to ^{3}MLCT and $^3\pi\pi^*$ respectively, matching assignments from the literature.[48-50]

To better explain these assignments, time-dependent density functional theory (TD-DFT) calculations were carried out for complexes **5** and **8** using the B3LYP hybrid density functional. The geometric parameters of the optimized structures (Tables S2 and S3) agree well with the experimental values. The molecular orbitals involved in the main excited states are depicted in Figures S13 and S14 and the relative compositions of

11

the different energy levels are reported in Table 5. Analysis of the frontier orbitals for **5** and **8** indicate that they are almost identical in both complexes. The HOMO and LUMO orbitals are predominantly ligand (CNC)-based with a moderate metallic contribution in the HOMO. As seen in Table 5 and in Figures S13 and S14, the HOMO is formed mainly by contributions of the phenyl rings of the CNC ligand [65% (**5**) and 60% (**8**)] and the Pt center [35% (**5**) and 40% (**8**)], whereas the LUMO is primarily located on the isonicotinic moiety of the CNC ligand (90% in **5** and 91% in **8**) and to a minor extent on the platinum center (5% in **5** and 6% in **8**) and the ancillary ligand (5% of CN-^{t}Bu in **5** and 4% of py-NH$_2$ in **8**). It is worth noting the participation of the ethylacetate group (R) in the frontier orbitals as is shown in the LUMO pictures (see Figures 6 and 7). Calculated excited states for **5** and **8** are listed in Table 6. The selected allowed transitions are in close agreement with the experimentally observed absorption maxima (Figures 6 and 7). TD-DFT calculations on **5** and **8** indicate that there is a considerable orbital mixing for the transitions and from those calculations, the lowest energy calculated absorptions are 371 and 364 nm respectively. These are involving the HO-2$\rightarrow$LUMO (91% for **5**) and HO-3$\rightarrow$LUMO (76% for **8**) transitions. As shown in Figures 6 and 7, the occupied orbitals implicated in these transitions (HO-2 for **5**) and (HO-3 for **8**) are the same. They are mostly constructed from orbitals located on the phenyl rings of the CNC tridentate ligand (92% in **5** and 90% in **8**) and also on the platinum center (8% in **5** and 10% in **8**). Thus, it seems that the lowest energy absorption in both complexes does not depend on the nature of the ancillary ligand but it corresponds to the intraligand (^{1}LC R-C^NC) transition mixed with some MLCT character. By analogy, in the rest of complexes, the lowest energy absorptions can be tentatively assigned to the same kind of transition. In addition, complex **8** shows a very weak calculated absorption at 417 nm (Figure 7) which involves the HO-2$\rightarrow$LUMO (97%) transition. As is observed in Figure S14, the HO-2 is mainly located on the dz^2 orbital of the platinum, which consequently may correspond to a ^{1}MLCT transition from the platinum center to the R-CNC ligand. These results agree well with the previous assignments made in the absorption spectroscopy section.

Emission Spectroscopy

The emission data for all the complexes are summarized in Table 7. All complexes are photoluminescent in solid state and in 2-Methyltetrahydrofuran (2-MeTHF) glassy solutions (77 K) except complexes **3**, **6** and **8** which are not emissive in solid state either

at 298 K or 77 K. None of them (**2**-**10**) are emissive in fluid solutions at room temperature. This is due to non-radiative processes concerning low lying d-d excited states and fast nonradiative decay rates, as a result of a large excited-state structural distortion.[66]

Solid state

In the solid state at room temperature, complex **2** shows a broad structured band with maxima at 608 nm which suffers minor modifications upon cooling to 77 K, giving well resolved vibronic spacings of 1311, 1307 cm^{-1} and slightly longer lifetimes. These vibronic progressions match the skeletal vibrational frequency of the R-C^N^C tridentate ligand and the lifetimes fit two different components suggesting the combined nature of the transition (see Figure 8 and Table 7). In line with previous assignments for similar complexes [Pt(R-C^N^C)(DMSO)],[50] we tentatively attribute these emissions to excimeric $^3\pi\pi^*$ excited states with a small contribution of ^{3}IL from the R-C^N^C ligand. Unlike compound **2**, the rest of the emissive complexes mentioned above show a very broad unstructured and rather weak emission band at 700 nm, except for **7** which does not exhibit any emissive behavior at room temperature (see Figure S15). Upon cooling to 77 K, the emissions became significantly enhanced, with narrowed bands but with hardly noteworthy bathochromic shifts (5 nm). Complex **7** displays a similar red emission centered at lower energies (735 nm) as shown in Figure 8. On the basis of their short lifetimes, minimal bathochromic shift and the absence of Pt-Pt interactions in crystal structures, these emissions are assigned to excited states derived from excimeric species or ground state aggregation of monomers.[36, 43, 44, 49-51, 54, 56, 68] According to the crystal structures and the solid state emissive behaviour of these compounds (**2**-**10**), it appears that complexes with a better overlap of the R-C^N^C ligands are not emissive in solid state. X-ray structures of **3**, **6** and **8** show rather short $\pi\pi$ contacts (3.30- 3.36 Å (**3**), 3.35 - 3.37 Å (**6**) and 3.37 - 3.50 Å (**8**)) with a very effective overlap of the aromatic rings in the PtCNC moiety and no emission was observed for any of them even at 77 K. However, complexes with barely any overlap of the CNC ligands, **4** (λ_{em} = 700 nm) and **9** (λ_{em} = 690 nm), are emitters at room temperature. Furthermore, solid state emissions for complexes **4** and **7** appear fairly red shifted from the similar ones in [Pt(C^N^C)(L)][49] and [Pt(Ph-C^N^C)(PPh$_3$)].[50] This could be caused by the different arrangements of the monomers in the solid state. There is evidence that the ethylacetate substituent at the back of the tridentate ligand is playing an important role in the self

assembly of the monomers into pairs and also in the supramolecular architecture (Figures S2 and 2).

Glassy state

In diluted glassy solutions (5 x 10^{-5} M, 77 K), complexes **2** and **3** exhibit the same emission behaviour (Figure 9). Both display structured bands with maxima at ~ 550 nm showing vibronic spacings of 1351 (**2**) and 1332 cm^{-1} (**3**) and lifetimes of a few microseconds. Emission profiles are not sensitive to the concentration (10^{-3} M) or the excitation wavelength, and they are very similar to the one observed for **2** in solid state at 77 K although rather narrow and shifted to higher energies. In contrast, complexes **4**-**10** show very different emission behaviour. All of them exhibit a highly structured band with maxima at 490 nm upon exciting in the 350-390 nm range. The vibrational spacings are ca. 1350-1500 cm^{-1} corresponding to C=C / C=N stretches of the (R-C^N^C) ligand. Besides this high energy band, complexes **5**, **9** and **10** revealed an additional band at very low energies (~ 700 nm) with shorter lifetimes; when exciting in the 370 nm range this become the major band (see Figure 10). Upon exciting with λ_{ex} > 420 nm there is a dramatic change in the emission profile, whereby a different structured band becomes predominant. This emission band appears at lower energies (~ 550 nm) with shorter lifetimes and it seems very similar to that observed in **2** and **3**. In this case, the emission band at very low energies (~ 700 nm) is barely observable whereas the high energy band at 491 nm is still visible (see Figure 10, red solid line). The rest of complexes (**4**, **6**-**8**) do not display this low energetic emission band (~ 700 nm) but they do show the structured bands at 490 and 550 nm upon exciting whether at 390 or 434 nm respectively (see Figure S16). These low-energy emissions (~ 700 nm), frequently encountered in Pt(II) complexes, are usually attributed to excimers or aggregates, therefore, the influence of the concentration was examined on complex **5**. As an illustrative example, Figure 11 shows the emission behavior of glassy solutions of complex **5** in 2-MeTHF at two different concentrations. In very dilute glassy solutions (10^{-5} M) the HE and (491 nm) and the LE (700 nm) bands can be enhanced by tuning the λ_{ex}. However, the 550 nm band is not visible at any excitation wavelength (see Figure 11). Interestingly, the 700 nm emission is still noticeable even in very dilute solutions, suggesting the excimeric origin for this transition. Concentrated glassy solutions gave similar emission spectra although there are a few differences. Both

14

bands, the HE (490 nm) and the LE (700 nm), are still dependant on the excitation wavelength but the HE one is no longer enhanced over the LE. The LE emission is the most significant over a wide range of excitation wavelengths. In addition, the 550 nm band, that was absent in very dilute solutions (10^{-5} M), appears when exciting at 420 nm. Therefore, from all these data, the 550 nm band, observed in 5 x 10^{-5} M glassy solutions of **2**-**10** ($\lambda_{ex} > 420$ nm), is attributed to $^3\pi\pi$ excited states due to the formation of aggregates in the ground state. The low energy excitations, the microsecond lifetimes and the fact that this band does not appear at very dilute solutions (10^{-5} M) supports this assignments The LE band (700 nm) observed in 5 x 10^{-5} M solutions of **5**, **9** and **10** (λ_{ex} ~ 370 nm) is attributed to $^3\pi\pi$ excimeric transitions by the collision of an excited molecule with another molecule during its luminescence lifetime.[107, 108] The diluted spectra showing no low energy excitations (Figures 10 and 11), the shorter lifetimes and the fact that the emission band (700 nm) is visible even at very diluted concentrations (10^{-5} M) support this assignment. Nonetheless, in highly concentrated solutions (10^{-3} M) it might form aggregates in the ground state because the excitation spectra is fairly different (Figure 11, down). Finally the HE band (490 nm) observed in 5 x 10^{-5} M solutions of **4**-**10** (λex < 390 nm) is assigned to metal perturbed intraligand $^3\pi\pi$ transitions, as it exhibit rather long lifetimes and a highly structured emission profile. Similar concentration-dependent behavior has been extensively reported for related complexes.[44, 48, 49, 65, 107]

Taking into account all these emission data values, complexes **5** and **9** might be considered to be potential phosphorescent components to fabricate WOLEDs because this type of excimeric platinum complexes would emit across the entire visible spectrum (Figure 10 and 11).[109, 110]

Concluding Remarks

A new family of bis-cyclometalated [Pt(EtOOC-C^N^C)(L)] complexes has been prepared and structurally and photophysically characterized. Crystal structures of the complexes (**2**-**10**) have been determined, showing in all cases, the existence of a variety of non-covalent interactions, although in no case were metal-metal contacts evident. The -CO$_2$Et substituent in the tridentate ligand is the directing force for arranging the

monomers into supramolecular networks. The absorption spectra of all of the species show metal perturbed intraligand absorptions which are not affected by the nature of the ancillary ligand. Complexes **3** and **6-10** show a shoulder at lower energies attributed to ^{1}MLCT. These assignments are supported by the TD-DFT calculations performed on complexes **5** and **8**. The participation of the ethylacetate group in the LUMO is particularly worthy of note. Solid state emission behavior is related to the structural features found in the solid state. Complexes with a better overlap of the R-CNC ligands are not emissive at room temperature (**3**, **6**, **7** and **8**). The remainder of the complexes show $^{3}\pi\pi*$ bands. Emissions in glassy solution are sensitive to excitation wavelength and the concentration. High energy bands due to intraligand transitions, emission bands originated by aggregates as well as the low energy ones which are assigned to excimeric excited states can be obtained by tuning the excitation wavelength and the concentration. Complexes **5** and **9** might be used as suitable phosphorescent emitters for WOLEDs because of their emission profile in glassy solutions. It covers a great range of visible spectrum. There is evidence that the CO_2Et substituent affects the solid state self assembly of the monomers and therefore the optical properties, based on the differences found between **4** and **7** and very similar complexes.[49-50]

Experimental Section

General Comments. Information describing materials, instrumental methods used for characterization, photophysical and spectroscopic studies, computational details concerning TD-DFT calculations and X-ray structures, as well as full NMR data are contained in the Supporting Information.

Preparation of (EtO$_2$C-C^N^C-H$_2$) (A). A mixture of 2,6-diphenyl isonicotinic acid (600 mg, 2.17 mmol), ethanol (10 mL), and concentrated sulphuric acid (0.1 mL) was refluxed over night, giving a clear solution. The volatiles were removed and the residue was treated with diethylether (4 x 30 mL). The combined diethyl ether solutions were washed with brine (30 mL) and water (30 mL) then dried with anhydrous MgSO$_4$ and evaporated to dryness. Yield: 486 mg (74%). Anal. Calcd for C$_{18}$H$_{13}$NO$_2$: C, 79.18; H, 5.64; N, 4.61. Found: C, 79.00; H, 5.63; N, 4.55. IR (ATR, cm^{-1}): ν(C=O) 1715(s).

Preparation of [{(EtO$_2$C-C^N^C-H)Pt(μ-Cl)}$_2$] (1). A modification of Rourke's method was employed.[47] A mixture of K$_2$PtCl$_4$ (300 mg, 0.72 mmol) and EtO$_2$C-C^N^C-H$_2$ (242 mg, 0.79 mmol) in glacial acetic acid (150 mL) was refluxed for 3 days. The mixture was filtered and the precipitate was washed with water (10 mL), methanol (5 mL) and diethylether (5 mL). The resulting solid was recrystallised from CH$_2$Cl$_2$/Et$_2$O to give pure **1** as a bright yellow solid. Yield: 180 mg, 46%. Anal. Calcd for C$_{40}$H$_{32}$N$_2$O$_4$Pt$_2$Cl$_2$: C, 45.08; H, 3.03; N, 2.63. Found: C, 44.54; H, 3.00; N, 2.50. IR (ATR, cm^{-1}): ν(C=O) 1726 (s). MS-ESI (+): m/z: 1029 [*M* - Cl]$^+$.

Preparation of [(EtO$_2$C-C^N^C)Pt(DMSO)] (2). A mixture of **1** (150 mg, 0.281 mmol) was dissolved in hot dimethyl sulfoxide (3 mL). Water (15 mL) and Na$_2$CO$_3$ (10 mg) were added to render an orange solid. After stirring for 1 h, the solid was collected by filtration and washed with water, acetone and diethyl ether. The crude product was recrystallized from CH$_2$Cl$_2$/Et$_2$O to give **2** as a pure solid. Yield: 143 mg (88%). Anal. Calcd for C$_{22}$H$_{21}$NO$_3$PtS: C, 46.00; H, 3.68; N, 2.44. Found: C, 46.20; H, 3.75; N, 2.38. IR (ATR, cm^{-1}): ν(C=O) 1716 (s). MS-ESI (+): m/z: 574 [*M*]$^+$.

Preparation of [(EtO$_2$C-C^N^C)Pt(tht)] (3). A mixture of **2** (200 mg, 0.34 mmol) and tetrahydrothiophene (tht) (90 μL, 1.02 mmol) in methanol (15 mL) was stirred at room temperature for 15 h. The resulting suspension was evaporated to 5 mL, filtered and the filtrate was washed with methanol to afford a deep orange solid. Yield: 187 mg (92%). Anal. Calcd for C$_{24}$H$_{23}$NO$_2$PtS: C, 49.30; H, 3.96; N, 2.39. Found: C, 49.00; H, 3.90; N, 2.24. IR (ATR, cm^{-1}): ν(C=O) 1728 (s). MS-ESI (+): m/z: 585 [*M*]$^+$.

Preparation of [(EtO₂C-C^N^C)Pt(PPh₃)] (4). PPh₃ (71 mg, 0.27 mmol) was added to a solution of **2** (155 mg, 0.27 mmol) in dichloromethane (15 mL). After stirring for 3 h at room temperature, the solvent was evaporated to dryness. Upon addition of methanol (10 mL) an orange solid was obtained which was collected by and filtration. Yield: 197 mg (96%). Anal. Calcd for $C_{38}H_{30}NO_2PPt$: C, 60.14; H, 3.98; N, 1.84. Found: C, 59.90; H, 4.01; N, 1.71. IR (ATR, cm^{-1}): ν(C=O) 1723 (s). MS-ESI (+): m/z: 759 $[M]^+$.

Preparation of [(EtO₂C-C^N^C)Pt(CN-*ᵗ*Bu)] (5). CN-*ᵗ*Bu (43 μL, 0.38 mmol) was added to a solution of **2** (200 mg, 0.34 mmol) in dichloromethane (15 mL). After stirring for 3 h at room temperature, the solvent was evaporated to dryness. Upon addition of diethyl ether (10 mL) an orange solid was obtained and air filtered. Yield: 167 mg (83%). Anal. Calcd for $C_{25}H_{24}N_2O_2Pt$: C, 51.81; H, 4.17; N, 4.83. Found: C, 51.80; H, 4.21; N, 4.73. IR (ATR, cm^{-1}): ν(C≡N) 2163 (s), ν(C=O) 1717 (s). MS-ESI (+): m/z: 580 $[M]^+$.

Preparation of [(EtO₂C-C^N^C)Pt(py)] (6). This compound was prepared following the method described for **5**. Pyridine (56 μL, 0.68 mmol) and **2** (200 mg, 0.34 mmol). **6** (178 mg, 88%). Anal. Calcd for $C_{25}H_{20}N_2O_2Pt$: C, 52.17; H, 3.50; N, 4.86. Found: C, 51.20; H, 3.59; N, 4.55. IR (ATR, cm^{-1}): ν(C=O) 1716 (s). MS-ESI (+): m/z: 576 $[M]^+$.

Preparation of [(EtO₂C-C^N^C)Pt(py-*ᵗ*Bu)] (7). This compound was prepared following the method described for **5**. 4-*tert*-Butylpyridine (153 μL, 1.02 mmol) and **2** (200 mg, 0.34 mmol). **7** (193 mg, 88%). Anal. Calcd for $C_{29}H_{28}N_2O_2Pt$: C, 55.13; H, 4.47; N, 4.43. Found: C, 55.00; H, 4.31; N, 4.10. IR (ATR, cm^{-1}): ν(C=O) 1724 (s). MS-ESI (+): m/z: 632 $[M]^+$.

Preparation of [(EtO₂C-C^N^C)Pt(py-NH₂)] (8). This compound was prepared following the method described for **5**. 4-Aminopyridine (41 mg, 0.43 mmol) and **2** (250 mg, 0.43 mmol). **8** (224 mg, 87%). Anal. Calcd for $C_{25}H_{21}N_3O_2Pt$: C, 50.83; H, 3.58; N, 7.11. Found: C, 50.20; H, 3.70; N, 6.80. IR (ATR, cm^{-1}): ν(C=O) 1707 (s). MS-ESI (+): m/z: 591 $[M]^+$.

Preparation of [(EtO₂C-C^N^C)Pt(py-CN)] (9). This compound was prepared following the method described for **5**. 4-Cyanopyridine (72 mg, 0.70 mmol) and **2** (200 mg, 0.35 mmol). **9** (179 mg, 84%). Anal. Calcd for $C_{26}H_{19}N_3O_2Pt$: C, 51.99; H, 3.19; N, 7.00. Found: C, 51.75; H, 3.11; N, 6.82. IR (ATR, cm^{-1}): ν(CN) 2234 (w); ν(C=O) 1707 (s).

Preparation of [(EtO₂C-C^N^C)Pt(py-CONH₂)] (10). Isonicotinamide (47 mg, 0.38 mmol) was added to a solution of **2** (200 mg, 0.35 mmol) in acetone (15 mL). After stirring for 16 h at room temperature, the solvent was evaporated to dryness. Addition of diethyl ether (2 x 5 mL) yielded an orange solid which was air filtered and washed with methanol (2 mL), dichloromethane (5 mL) and Et₂O (10 mL). Yield: 194 mg (89%). Anal. Calcd for

$C_{26}H_{21}N_3O_3Pt$: C, 50.47; H, 3.42; N, 6.79. Found: C, 50.10; H, 3.53; N, 6.78. IR (ATR, cm^{-1}): ν(C=O) 1688 (s, br, COOEt, CONH$_2$). MS-ESI (+): m/z: 619 [M]$^+$.

Supporting information available: General procedures and materials, computational details, crystallographic details, scheme S1 and full NMR data. Xray structure analysis of **3**-**10** (Table S1 and Fig. S1-S8). ^{1}H NMR of **8** at 203 K (Fig. S9). Normalized UV-Vis spectra of complexes **6**-**10** in dichloromethane (Fig. S10-S12). Tables of atomic coordinates of compounds **5** and **8** (S2, S3) and pictures of the representative frontier orbitals for them (Fig. S13 and S14). Solid state emission spectra (Fig. S15) and normalized spectra of 2-MeTHF glassy solutions of **5** at different concentrations (Fig. S16).
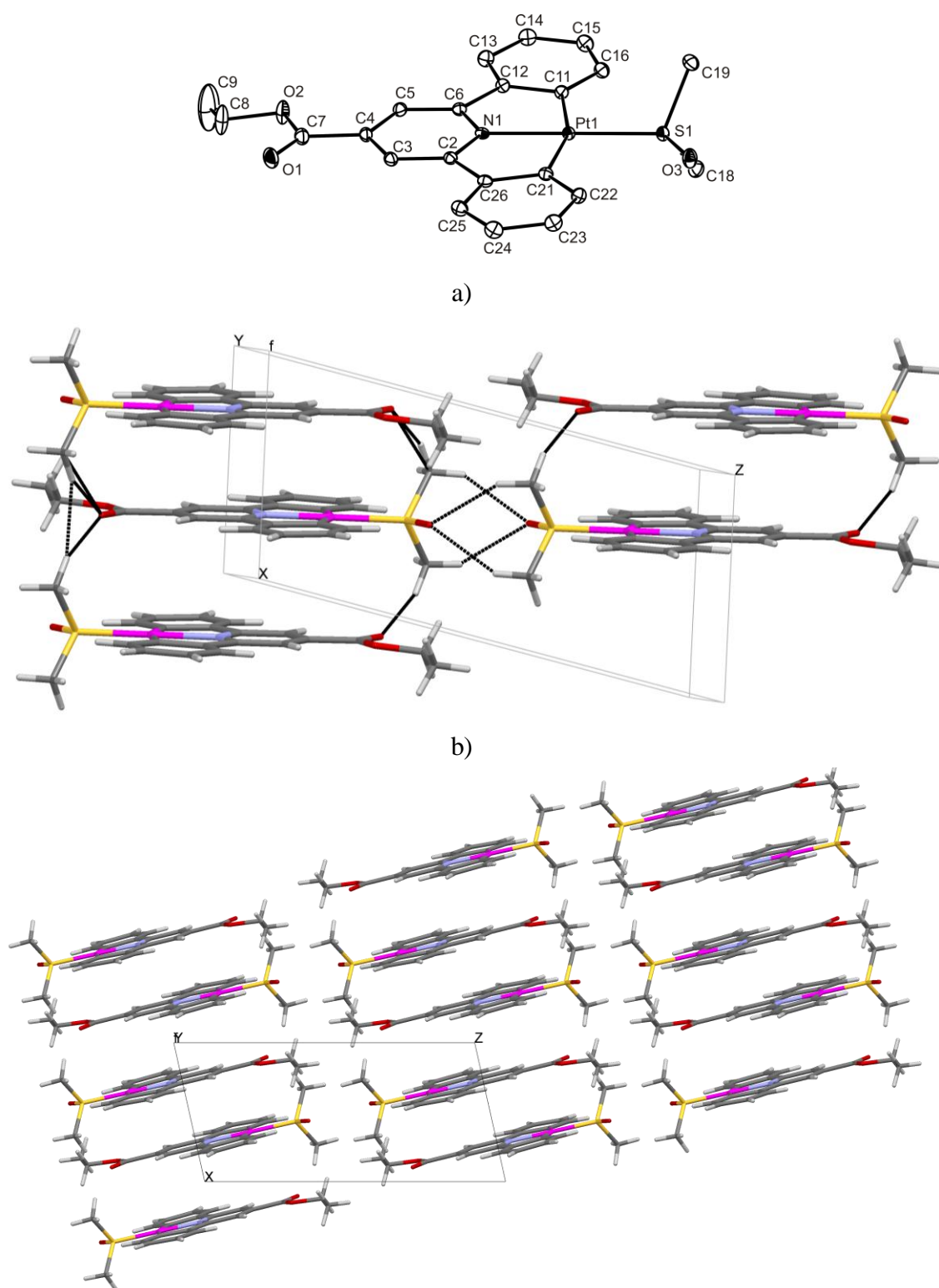
Crystallographic data in CIF format.

Figure 1. a) ORTEP view of **2**. Ellipsoids are drawn at the 30% probability level. Hydrogen atoms and solvent molecules have been omitted for clarity. b) Perspective view of the head to tail stacking arrangement. c) Crystal packing view along b (y) axis.
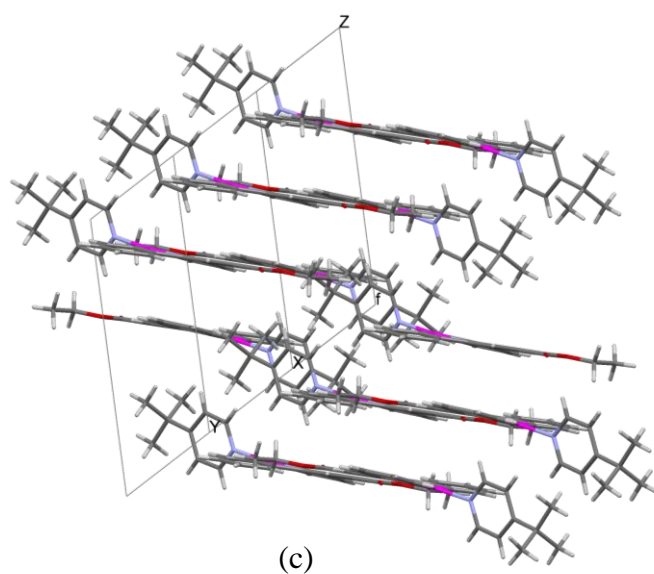
(a)

(b)

(c)
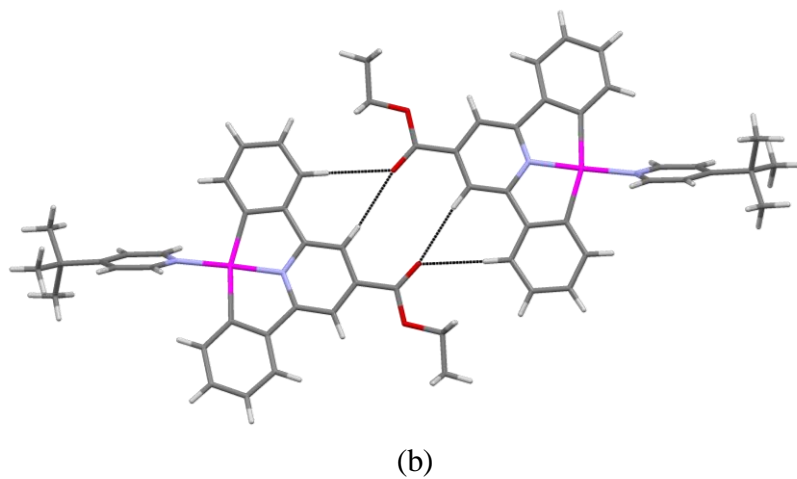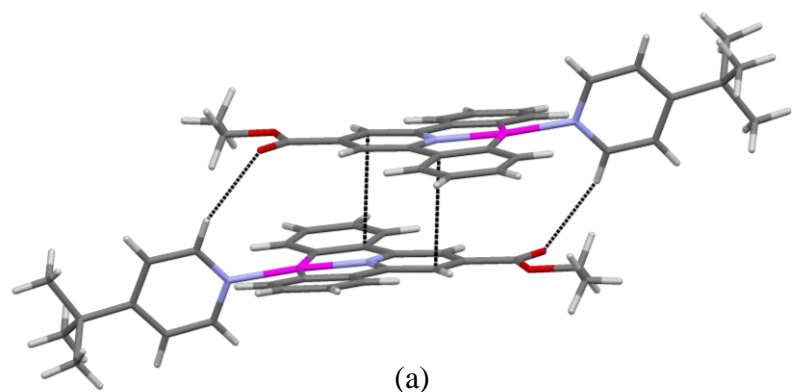
Figure 2. a) Head to tail molecular pairs of **7** showing close $\pi\cdots\pi$ and C-H (py)$\cdots$O (ester) contacts; b) Perspective view of monomers within the same layer showing C-H $\cdot\cdot$O contacts; c) Crystal packing diagram.

(a)

(b)

(c)

Figure 3. a) ORTEP view of **8**. Ellipsoids are drawn at the 50% probability level. Hydrogen atoms and solvent molecules have been omitted for clarity; b) Head to tail molecular pairs. c) Diagram showing further weak interactions.

a)
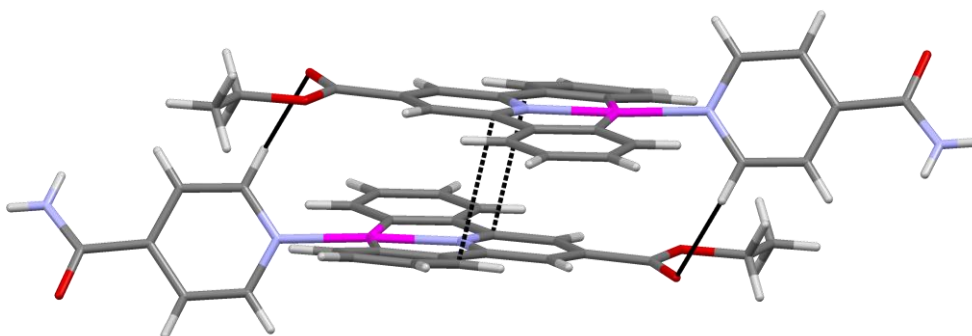
b)
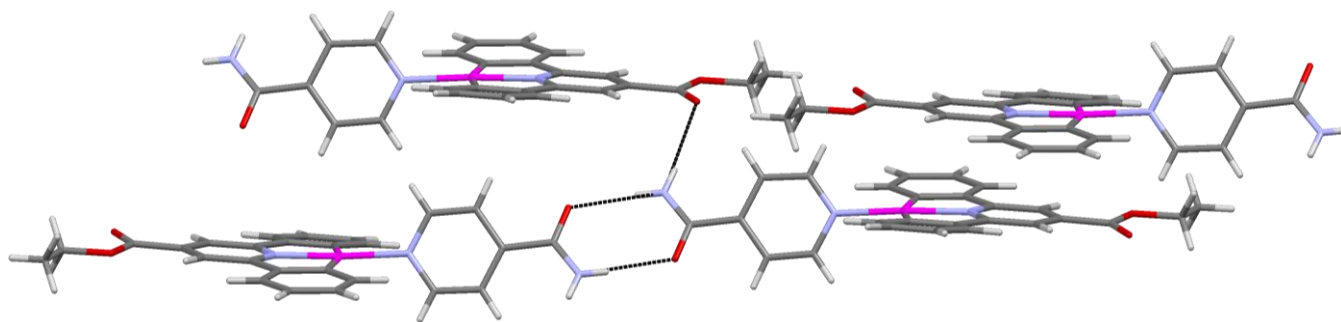
(c)

Figure 4. a) ORTEP view of **10**. Ellipsoids are drawn at the 50% probability level. Hydrogen atoms and solvent molecules have been omitted for clarity; b) Head to tail molecular pairs. c) Diagram showing the hydrogen bonding interactions of the molecules.
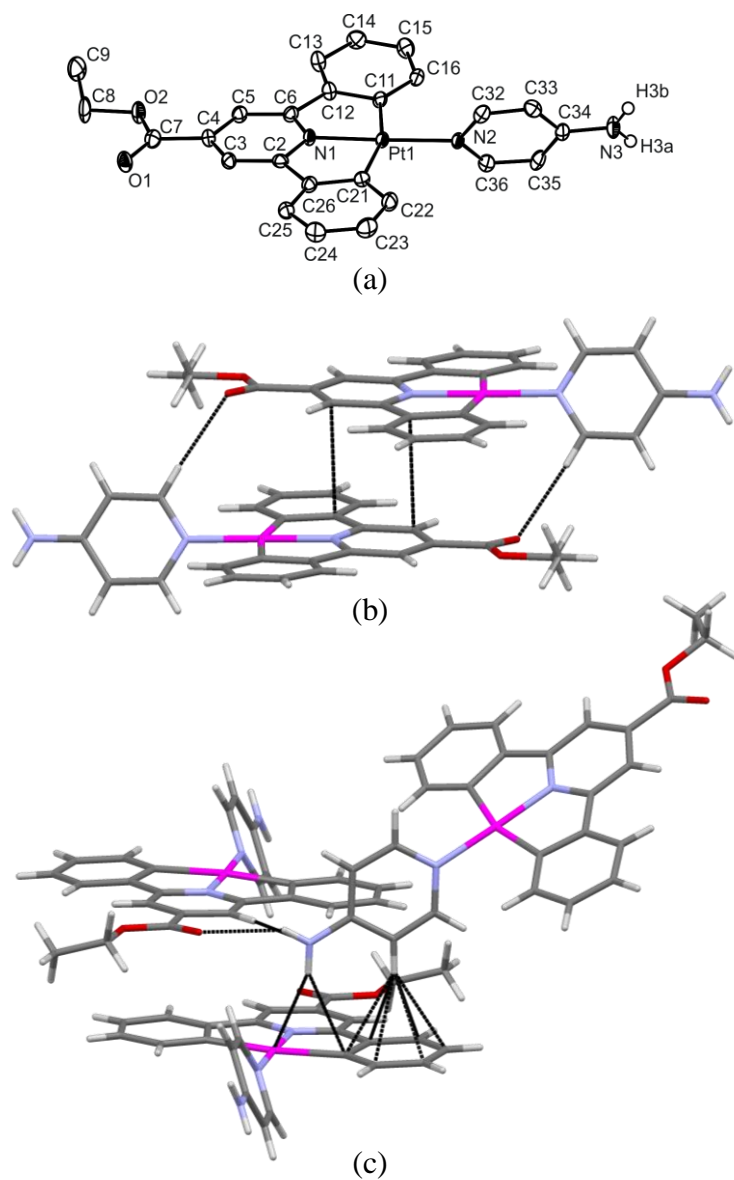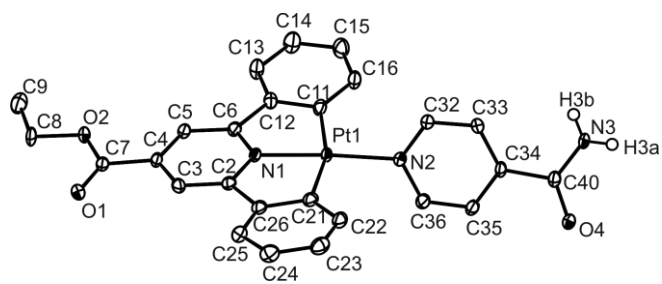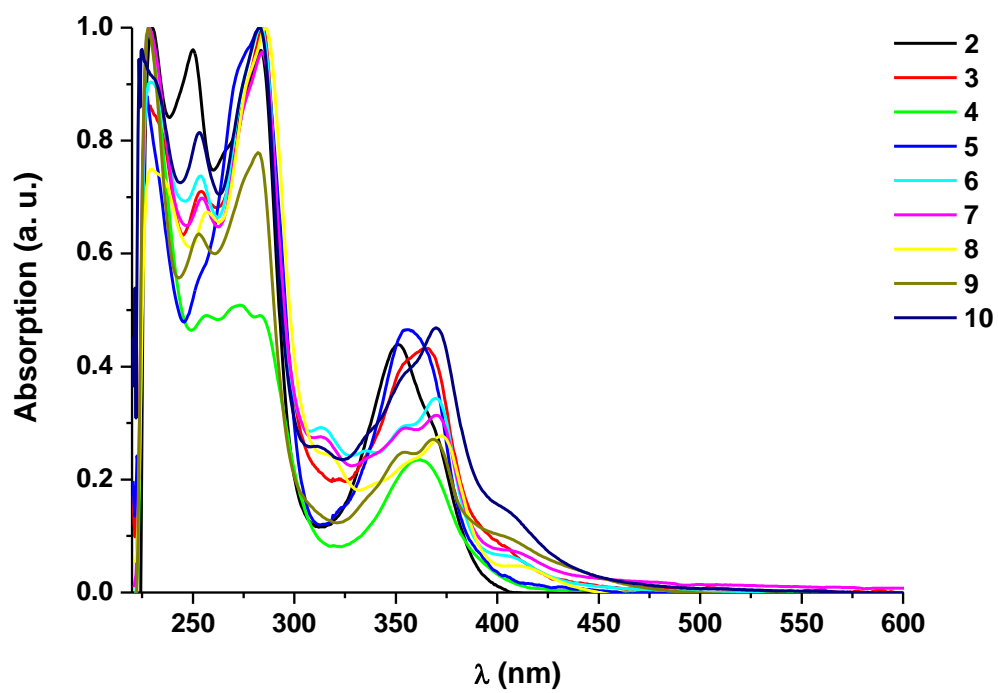
Figure 5. UV-Vis absorption spectra of complexes **2**-**10** in CH_2Cl_2 (10^{-5} M) at 298 K.
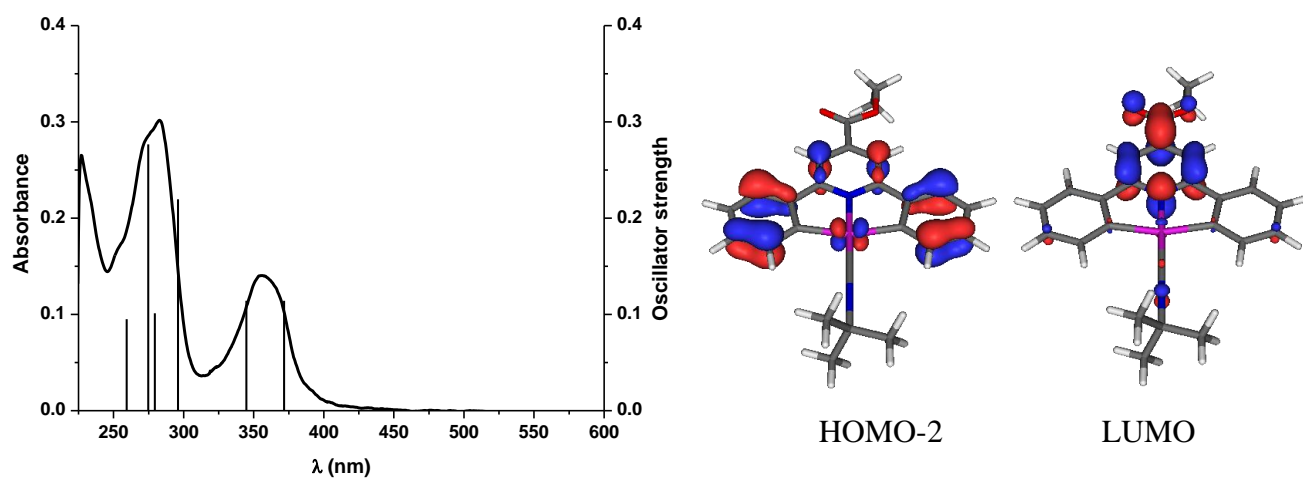
Figure 6. Left: calculated absorption spectra (bars) of **5** and experimental UV-Vis spectra in dichloromethane (10^{-5} M) at 298 K. Right: Frontier orbital plots for **5** obtained by DFT.
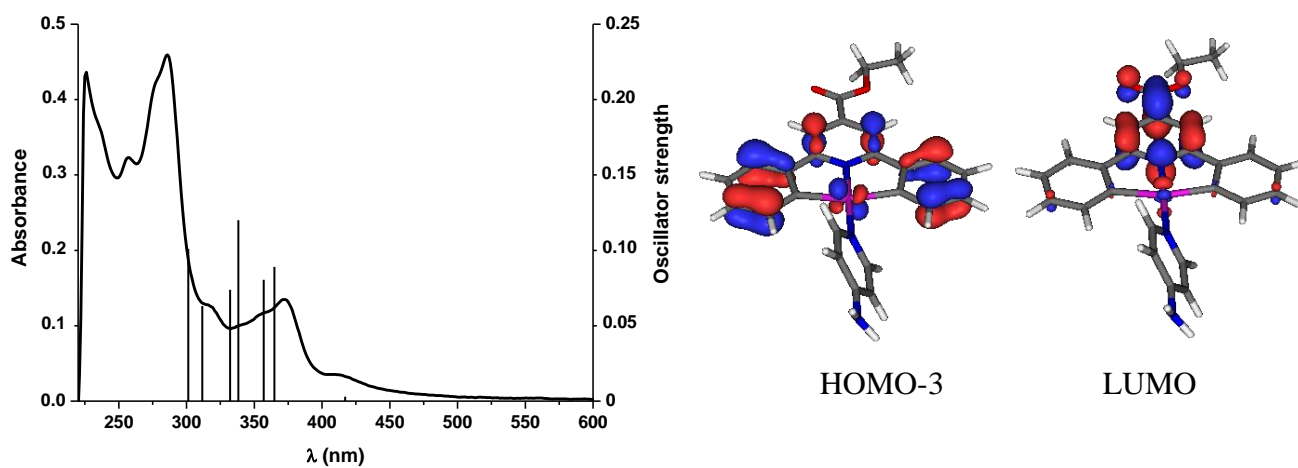
Figure 7. Left: calculated absorption spectra (bars) of **8** and experimental UV-Vis spectra in dichloromethane (10^{-5} M) at 298 K. Right: Frontier orbital plots for **8** obtained by DFT.
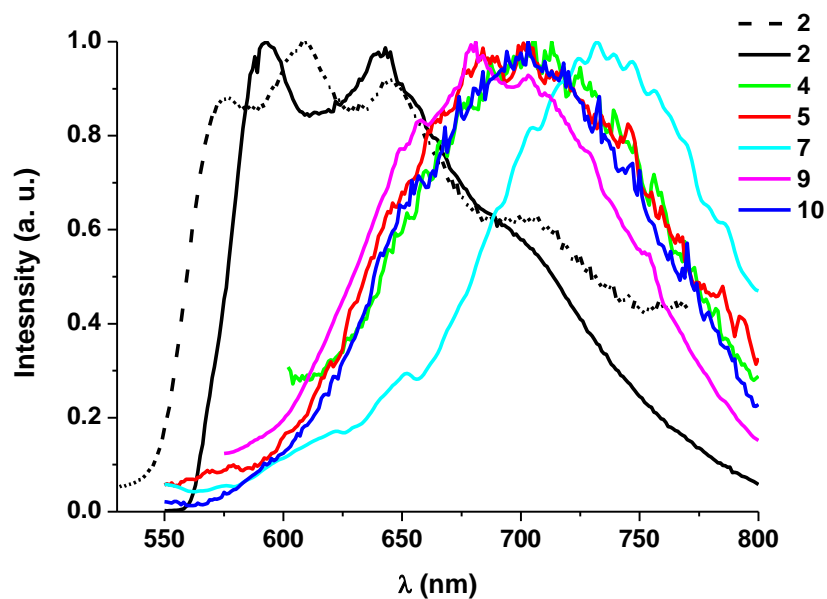
Figure 8. Normalized solid state emission spectra at 298 K (---) and 77 K (——).
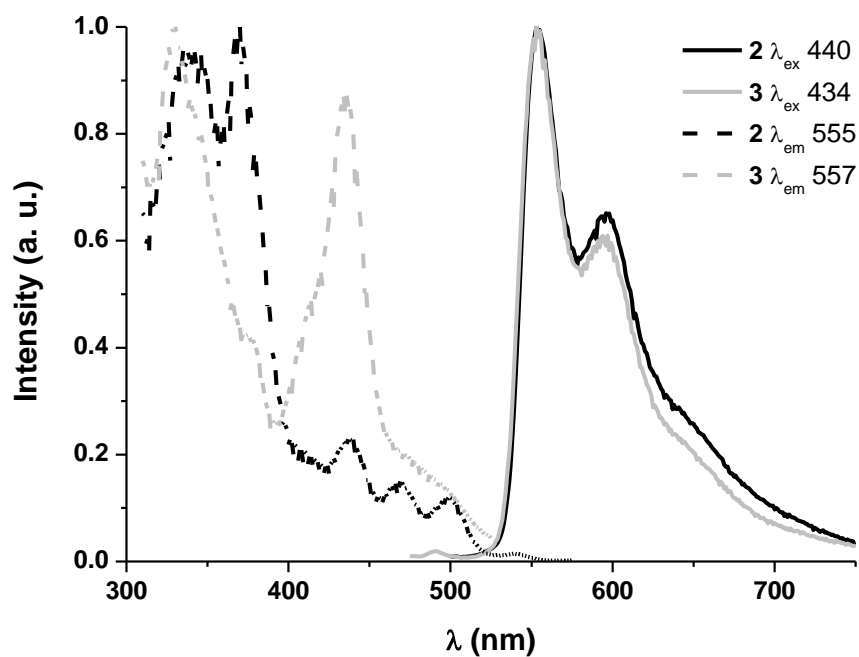
Figure 9. Normalized excitation and emission spectra of **2** and **3** in 2-MeTHF (5 x 10^{-5} M) at 77 K

Figure 10. Normalized excitation and emission spectra of **9** in 2-MeTHF (5 x 10^{-5} M) at 77 K

Figure 11. Normalized spectra of glassy (77 K) solutions of **5** in 2-MeTHF at 10^{-3} M (down) and 10^{-5} M (up).
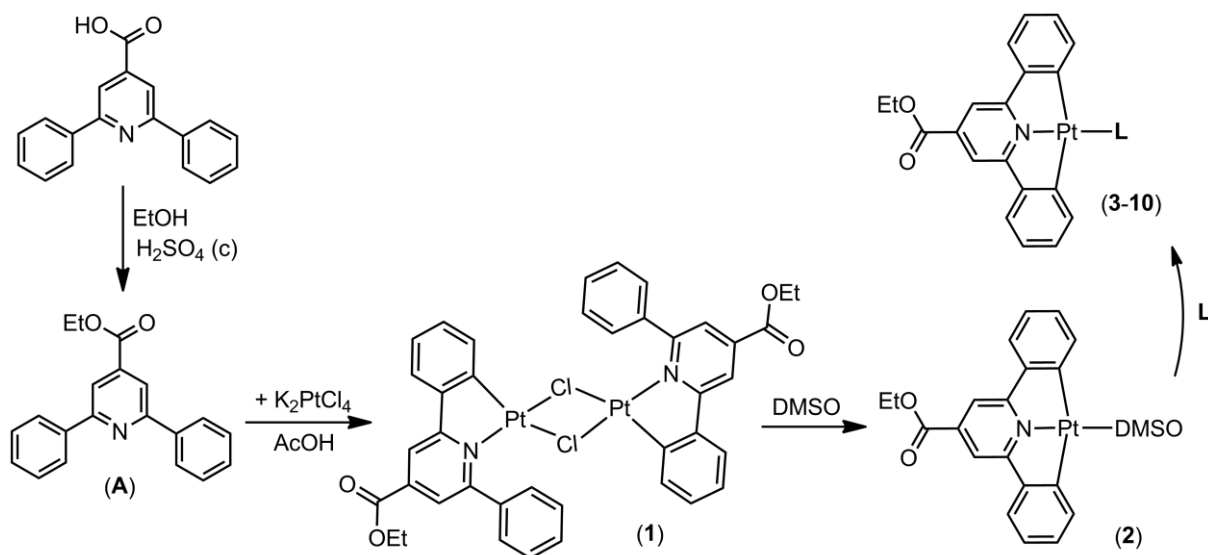
L= tht (**3**); PPh$_3$ (**4**); CN-*t*-Bu (**5**); py (**6**); py-^{t}Bu (**7**); py-NH$_2$ (**8**); py-CN (**9**); py-CONH$_2$ (**10**)

Scheme 1

Table 1. Crystallographic data for complexes **2-6**

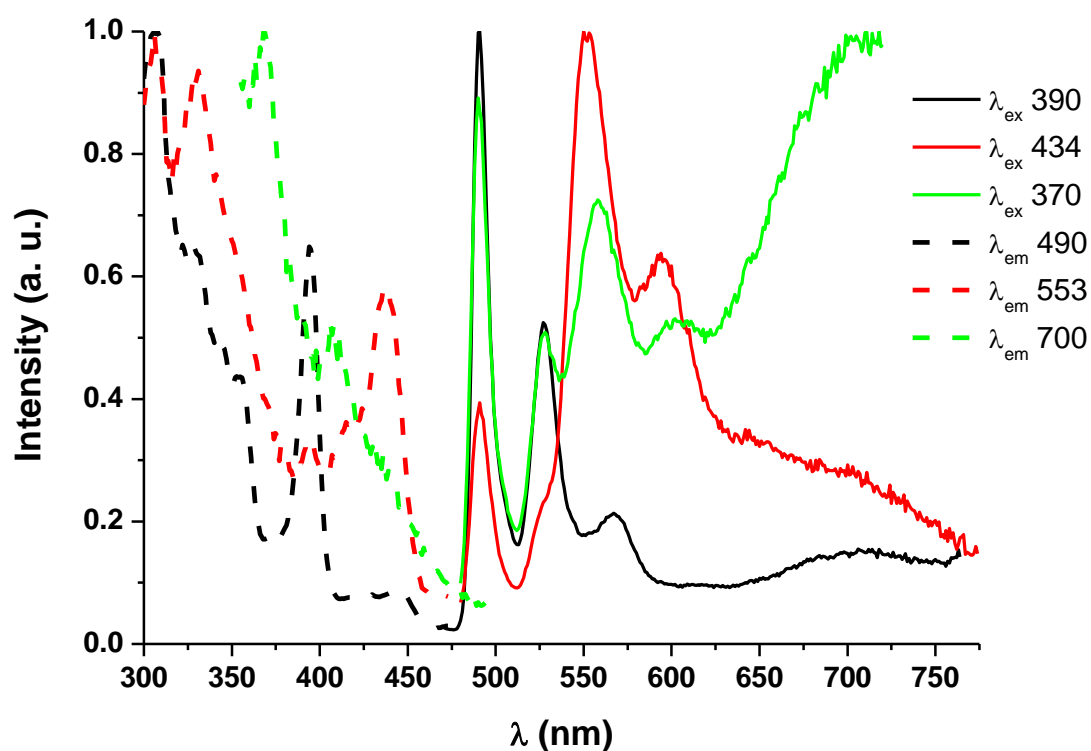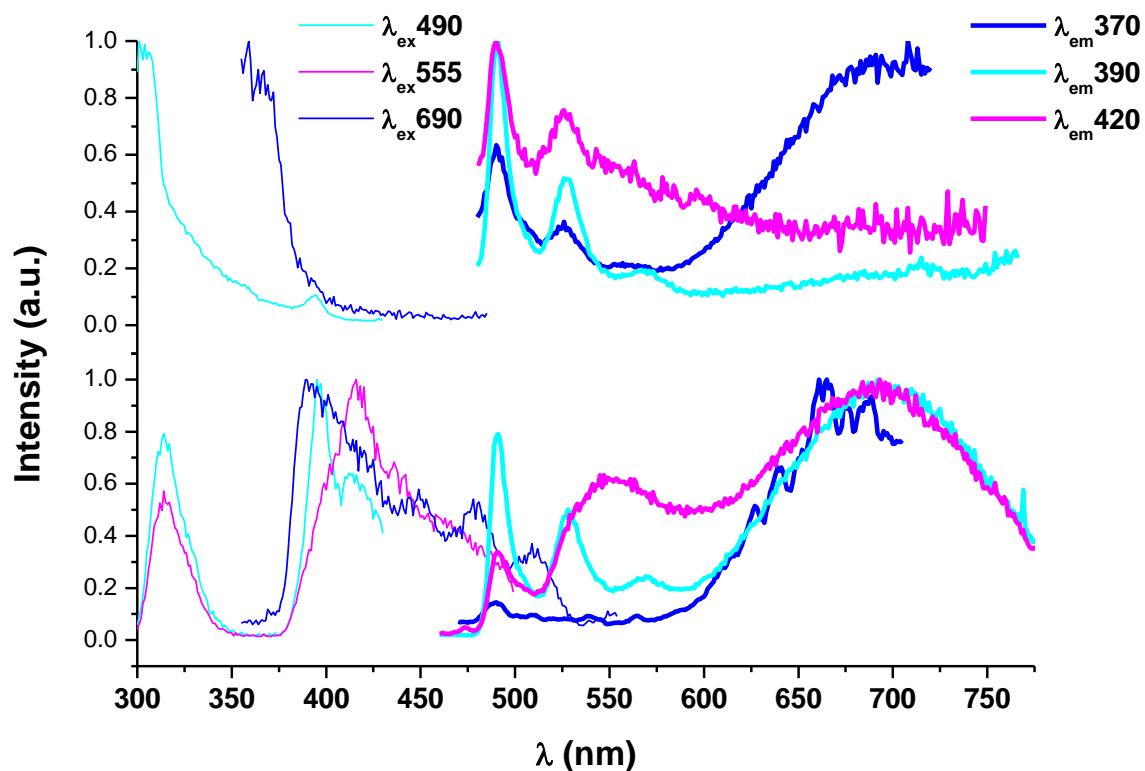|	2 CH$_2$Cl$_2$	3	4	5 CH$_2$Cl$_2$	6
Empirical formula	C$_{23.5}$H$_{24}$Cl$_3$NO$_3$PtS	C$_{24}$H$_{23}$NO$_2$PtS	C$_{38}$H$_{30}$NO$_2$PPt	C$_{26}$H$_{26}$Cl$_2$N$_2$O$_2$Pt	C$_{25}$H$_{20}$N$_2$O$_2$Pt
Formula weight	701.94	584.58	758.69	664.48	575.52
Crystal system	Triclinic	Monoclinic	Monoclinic	Monoclinic	Orthorhombic
Space group	*P* -1	*P* 1 21/*c* 1	*P* 1 21/*c* 1	*P* 1 21/*c* 1	*P b c a*
a (Å)	6.8179(1)	10.2790(10)	17.8659(3)	14.1871(2)	12.4337(1)
b (Å)	12.9134(2)	19.6900(2)	17.1383(2)	9.4268(1)	16.8711(1)
c (Å)	14.4381(2)	10.9680(10)	9.7579(1)	18.6910(2)	19.1912(1)
α (°)	88.678(1)	90	90	90	90
β (°)	77.306(1)	111.43(10)	101.968(1)	102.419(1)	90
γ (°)	85.367(1)	90	90	90	90
Volume (Å^3) / Z	1236.0(3) / 2	2066.4 (3)/ 4	2922.8 4(7)/ 4	2441.22(5) / 4	4025.74(5) / 8
Density (calculated) (Mg/m^3)	1.886	1.879	1.724	1.808	1.899
Absorption coefficient (mm^{-1})	6.111	6.912	4.893	5.993	6.996
F(000)	682	1136	1496	1296	2224
Crystal size (mm)	0.30 x 0.26 x 0.12	0.28 x 0.14 x 0.05	0.26 x 0.16 x 0.04	0.19 x 0.14 x 0.06	0.32 x 0.24 x 0.22
Theta range (°)	3.56 - 36.32	3.56 - 30.51	2.89 - 32.71	2.92 - 32.63	4.09 - 36.32
Reflections collected	62173	63109	59733	35909	122240
Independent reflections [R(int)]	11737 [0.0432]	6295[0.0271]	10203[0.0240]	8365[0.0291]	9734[0.0612]
Max. and min. transmission	1.000 and 0.490	0.731 and 0.242	0.840 and 0.437	1.000 and 0.602	0.349 and 0.246
Goodness-of-fit on F^2	1.057	1.086	0.975	1.045	0.993
Final R$_1$, wR$_2$ [I>2σ(I)]	0.0297, 0.0731	0.0187, 0.0435	0.0165, 0.0368	0.0217, 0.0412	0.0271, 0.0762
R$_1$, wR$_2$ (all data)	0.0398, 0.0781	0.0223, 0.0448	0.0252, 0.0375	0.0313, 0.0437	0.0429, 0.0797
Largest diff. peak, hole/e.Å^{-3}	1.810 and -4.045	2.988, -0.757	1.066, -0.608	1.207 and -1.048	2.022 and -2.216

Table 2. Crystallographic data for complexes **7-10**

	7	8 CH$_2$Cl$_2$	9	10 2(CH$_2$Cl$_2$)
Empirical formula	C$_{29}$H$_{28}$N$_2$O$_2$Pt	C$_{26}$H$_{23}$Cl$_2$N$_3$O$_2$Pt	C$_{26}$H$_{19}$N$_3$O$_2$Pt	C$_{28}$H$_{25}$Cl$_4$N$_3$O$_3$Pt
Formula weight	631.62	675.46	600.53	788.40
Crystal system	Triclinic	Monoclinic	Monoclinic	Triclinic
Space group	*P* -1	*P* 1 21/*n* 1	*P* 1 21/*n* 1	*P* -1
a (Å)	8.6021(1)	12.3157(2)	10.5452(2)	10.5280(2)
b (Å)	12.1749(3)	12.2156(2)	27.6064(5)	12.2449(3)
c (Å)	13.2392(3)	16.2772(3)	7.3885(1)	13.0739(3)
α (°)	115.847(3)	90	90	65.409(2)
β (°)	104.631(2)	93.757(2)	100.074(2)	68.455(2)
γ (°)	90.247(2)	90	90	86.553(2)
Volume (Å^3) / Z	1196.89(4) / 2	2443.54(7) / 4	2117.74(6) / 4	1416.88(5) / 2
Density (calculated) (Mg/m^3)	1.753	1.836	1.884	1.848
Absorption coefficient (mm^{-1})	5.891	5.990 mm^{-1}	6.655	5.365
F(000)	620	1312	1160	768
Crystal size (mm)	0.40 x 0.27 x 0.21	0.14 x 0.08 x 0.02	0.43 x 0.28 x 0.20	0.19 x 0.08 x 0.03
Theta range (°)	2.90 - 32.71	3.32 - 28.28	2.86 - 32.71	2.93 - 32.89
Reflections collected	23107	16616	25666	28188
Independent reflections [R(int)]	8080[0.0218]	5971[0.0355]	7286[0.0494]	9606[0.0289]
Max. and min. transmission	0.3709 and 0.2016	0.856 and 0.592	0.319 and 0.138	0.846 and 0.544
Goodness-of-fit on F^2	0.958	0.803	1.016	0.947
Final R$_1$, wR$_2$ [I>2σ(I)]	0.0169, 0.0319	0.0226, 0.0328	0.0301, 0.0755	0.0220, 0.0422
R$_1$, wR$_2$ (all data)	0.0215, 0.0323	0.0420, 0.0340	0.0350, 0.0770	0.0315, 0.0430
Largest diff. peak, hole/e.Å^{-3}	1.132 and -0.743	0.895 and -0.922	3.659 and -1.755	1.246 and -1.026

Table 3. Selected bond lengths (Å) and angles (º) for **2** 3CH₂Cl₂

Distances (Å)			
Pt(1)-C(11)	2.088(3)	Pt(1)-C(21)	2.062(2)
Pt(1)-N(1)	2.014(2)	Pt(1)-S(1)	2.019(6)
C(4)-C(7)	1.491(4)	C(8)-C(9)	1.462(16)
C(7)-O(1)	1.209(4)	C(7)-O(2)	1.321(4)

Angles (º)			
C(11)-Pt(1)-C(21)	160.54(10)	C(11)-Pt(1)-S(1)	100.12(7)
N(1)-Pt(1)-C(21)	80.32(9)	C(21)-Pt(1)-S(1)	99.34(7)
N(1)-Pt(1)-C(11)	80.22(9)	Pt(1)-S(1)-O(3)	120.71(9)

Table 4. Absorption Data in CH₂Cl₂ solutions (10^{-5} M) for compounds **2-10** at RT

Compound	λ abs / nm (10^3 ε/M⁻¹cm⁻¹)
[Pt(R-C^N^C)DMSO] (**2**)	230 (39.7), 250 (38.1), 283 (38.1), 351 (17.4), 365 (sh, 11.8), 465 (0.6), 492 (0.4)
[Pt(R-C^N^C)tht] (**3**)	227 (26.7), 254 (21.9), 284 (30.9), 355 (12.5), 365 (13.3), 404 (sh, 2.6), 470 (0.2), 504 (0.2)
[Pt(R-C^N^C)PPh₃] (**4**)	228 (65.1), 257 (31.9), 273 (33.1), 283 (31.9), 362 (15.1), 472 (0.2), 503 (sh, 0.1)
[Pt(R-C^N^C)CN^{t}Bu] (**5**)	227 (26.5), 254 (sh, 17.0), 275 (28.6), 283 (30.1), 355 (14.0), 366 (12.7), 477 (0.2), 503 (0.1)
[Pt(R-C^N^C)py] (**6**)	229 (53.5), 254 (43.6), 283 (59.1), 313 (17.3), 355 (17.4), 370 (20.3), 402 (sh, 3.9), 510 (0.2), 550 (0.1)
[Pt(R-C^N^C)py-^{t}Bu] (**7**)	228 (54.8), 255 (38.3), 284 (52.5), 315 (15.0), 355 (15.9), 370 (17.2), 406 (sh, 4.1), 511 (0.2), 550 (0.1)
[Pt(R-C^N^C)py-NH₂] (**8**)	229 (69.6), 257 (62.6), 286 (92.9), 315 (22.8), 358 (21.8), 372 (25.7), 410 (sh, 4.3), 515 (0.2), 552 (0.1)
[Pt(R-C^N^C)py-CN] (**9**)	228 (51.4), 253 (32.6), 282 (40.0), 355 (12.8), 369 (13.9), 402 (sh, 5.3), 556 (0.1)
[Pt(R-C^N^C)py-CONH₂] (**10**)	225 (50.9), 253 (43.1), 252 (52.9), 310 (13.7), 356 (20.8), 370 (24.8), 402 (sh, 8.0), 513 (0.3), 551 (0.1)

Table 5. Population Analysis (%) of Frontier MOs in the Ground State for **5** and **8**.

MO	[(R-C^N^C)Pt(CN^{t}Bu)] (5)			[(R-C^N^C)Pt(py-NH$_2$)] (8)		
	Pt	R-C^N^C	CN-^{t}Bu	Pt	R-C^N^C	py-NH$_2$
LU+3	6	82	12	2	12	86
LU+2	14	67	19	4	6	90
LU+1	1	99	0	2	88	10
LUMO	5	90	5	6	91	3
HOMO	35	65	0	40	60	0
HO-1	19	73	7	26	65	9
HO-2	8	92	0	93	4	3
HO-3	95	4	1	10	90	0
HO-4	5	94	0	39	57	4
HO-5	12	84	4	20	75	5
HO-6	63	25	13	28	60	11
HO-7				49	27	24
HO-9	100	0	0			

Table 6. Selected singlet excited states calculated by TD-DFT for complexes **5** and **8**.

λ_{exc} (calc.)/nm	o.s.	Transition (Percentage contribution)
		[(R-C^N^C)Pt(CN^{t}Bu)] (5)
371.73	0.1141	HO-2 → LUMO (91%)
344.73	0.0669	HOMO → LU+1 (74%); HO-5 → LUMO (10%); HO-6 → LUMO (7%)
296.07	0.2196	HO-6 → LUMO (70%); HO-2 → LU+1 (18)
279.45	0.1011	HO-4 → LU+1 (52%); HO-9→ LUMO (20%); HO-1 → LU+2 (6%); HOMO → LU+2 (5%)
274.70	0.2767	HO-2→ LU+1 (67%); HO-6 → LUMO (11%); HOMO → LU+1 (5%)
259.35	0.0951	HOMO → LU+3 (61%); HO-5 → LU+1 (22%)
		[(R-C^N^C)Pt(py-NH$_2$)] (8)
417.05	0.0029	HO-2 → LUMO (97%)
364.79	0.0890	HO-3 → LUMO (76%); HOMO → LU+2 (13%)
356.90	0.0805	HOMO → LU+1 (48%); HO-4 → LUMO (32%); HOMO → LU+3 (6%)
338.26	0.1199	HO-5 → LUMO (87%); HO-5 → LUMO (3%)
332.23	0.0738	HO-1 → LU+2 (88%); HO-5 → LUMO (2%)
311.60	0.0632	HO-6 → LUMO (56%); HO-7 → LUMO (32%)
301.32	0.1020	HO-7 → LUMO (53%); HO-6 → LUMO (23%); HO-3 → LU+1 (8%); HO-4 → LU+2 (3%);

Table 7: Emission Data for complexes **2**-**10**

Compound	Media (T/K)	λ_{em} (nm)	τ (μs)
2	Solid (298)	575, 608$_{max}$, 646, 704$_{sh}$ (λ_{ex} 430)	0.1 (95%), 93.3 (5%)
	Solid (77)	593$_{max}$, 643, 702$_{sh}$ (λ_{ex} 400-550)	1.0 (92%), 125.1 (8%)
	2-MeTHF$_d$ (77)	555$_{max}$, 600, 642$_{sh}$ (λ_{ex} 340-500)	7.01
3	2-MeTHF$_d$ (77)	553$_{max}$, 597, 641$_{sh}$ (λ_{ex} 434)	6.8
4	Solid (298)	700 (λ_{ex} 430)	a
	Solid (77)	705 (λ_{ex} 430-550)	0.26
	2-MeTHF$_d$ (77)	491$_{max}$, 528, 565, 620 (λ_{ex} 360-390)	
		491, 528, 556$_{max}$, 600 (λ_{ex} 420-440)	
5	Solid (298)	690 (λ_{ex} 430)	a
	Solid (77)	700 (λ_{ex} 475)	0.45
	2-MeTHF$_d$ (77)	490$_{max}$, 527, 569, 690 (λ_{ex} 350-390)	27.2 (490),
		490, 527, 555, 600$_{sh}$ (λ_{ex} 420-440)	2.8 (550)
	2-MeTHF$_c$ (77)	491, 530, 571, 696$_{max}$ (λ_{ex} 350-390)	0.6 (696)
		490, 552, 695$_{max}$ (λ_{ex} 420-440)	
6	2-MeTHF$_d$ (77)	491$_{max}$, 528, 566 (λ_{ex} 390)	25.0 (491)
		490, 528$_{sh}$, 553$_{max}$, 597(λ_{ex} 410-440)	3.6 (553)
7	Solid (77)	735 (λ_{ex} 420-550)	a
	2-MeTHF$_d$ (77)	491$_{max}$, 528, 566 (λ_{ex} 390)	
		490, 528$_{sh}$, 553$_{max}$, 597(λ_{ex} 410-440)	
8	2-MeTHF$_d$ (77)	491$_{max}$, 528, 566 (λ_{ex} 390)	
		490, 528$_{sh}$, 553$_{max}$, 597(λ_{ex} 410-440)	
9	Solid (298)	690 (λ_{ex} 475)	a
	Solid (77)	694 (λ_{ex} 410-550)	0.49
	2-MeTHF$_d$ (77)	491$_{max}$, 528, 566, 700 (λ_{ex} < 390)	27.6 (491)
		490, 528$_{sh}$, 553$_{max}$, 597(λ_{ex} 410-440)	4.0 (553)
10	Solid (298)	695 (λ_{ex} 450)	a
	Solid (77)	700 (λ_{ex} 420-550)	0.11
	2-MeTHF$_d$ (77)	491$_{max}$, 528, 566, 700 (λ_{ex} < 390)	26.1 (491)
		490, 528$_{sh}$, 553$_{max}$, 597(λ_{ex} 410-440)	7.0 (553)

a = too weak to be measured; c = 10^{-3}M; d = 5 x 10^{-5}M;

References

1. Williams, J. A. G., *Top Curr Chem*, **2007**, *281*, 205-268.
2. Maestri, M.;Deuschel-Cornioley, C. and von Zelewsky, A., *Coord. Chem. Rev.*, **1991**, *111*, 117-123.
3. Balashev, K. P.;Puzyk, M. V.;Kotlyar, V. S. and Kulikova, M. V., *Coord. Chem. Rev.*, **1997**, *159*, 109-120.
4. Gareth Williams, J. A.;Develay, S.;Rochester, D. L. and Murphy, L., *Coord. Chem. Rev.*, **2008**, *252*, 2596-2611.
5. Murphy, L. and Williams, J. A. G., in *Molecular Organometallic Materials for Optics*, eds. H. LeBozec and V. Guerchais, Springer-Verlag Berlin, 2010, pp. 75-111.
6. Wong, W. Y., *Journal of Organometallic Chemistry*, **2009**, *694*, 2644-2647.
7. Chong, S. H. F.;Lam, S. C. F.;Yam, V. W. W.;Zhu, N. Y.;Cheung, K. K.;Fathallah, S.;Costuas, K. and Halet, J. F., *Organometallics*, **2004**, *23*, 4924-4933.
8. Chen, Y.;Li, K.;Lu, W.;Chui, S. S.-Y.;Ma, C.-W. and Che, C.-M., *Angewandte Chemie International Edition*, **2009**, *48*, 9909-9913.
9. Sotoyama, W.;Satoh, T.;Sawatari, N. and Inoue, H., *Appl. Phys. Lett.*, **2005**, *86*.
10. Wong, W. Y. and Ho, C. L., *Accounts Chem. Res.*, **2010**, *43*, 1246-1256.
11. Wong, W. Y.;Chow, W. C.;Cheung, K. Y.;Fung, M. K.;Djurisic, A. B. and Chan, W. K., *Journal of Organometallic Chemistry*, **2009**, *694*, 2717-2726.
12. Zhao, Q.;Li, F. and Huang, C., *Chemical Society Reviews*, **2010**, *39*, 3007-3030.
13. Yam, V. W. W.;Tang, R. P. L.;Wong, K. M. C.;Lu, X. X.;Cheung, K. K. and Zhu, N. Y., *Chem.-Eur. J.*, **2002**, *8*, 4066-4076.
14. Taylor, S. D.;Howard, W.;Kaval, N.;Hart, R.;Krause, J. A. and Connick, W. B., *Chem. Commun.*, **2010**, *46*, 1070-1072.
15. Ma, D. L. and Che, C. M., *Chem.-Eur. J.*, **2003**, *9*, 6133-6144.
16. Ma, D.-L.;Shum, T. Y.-T.;Zhang, F.;Che, C.-M. and Yang, M., *Chem. Commun.*, **2005**, 4675-4677.
17. Wu, P.;Wong, E. L. M.;Ma, D. L.;Tong, G. S. M.;Ng, K. M. and Che, C. M., *Chem.-Eur. J.*, **2009**, *15*, 3652-3656.
18. Ma, D. L.;Che, C. M. and Yan, S. C., *Journal of the American Chemical Society*, **2009**, *131*, 1835-1846.
19. Koo, C. K.;Wong, K. L.;Man, C. W. Y.;Lam, Y. W.;So, K. Y.;Tam, H. L.;Tsao, S. W.;Cheah, K. W.;Lau, K. C.;Yang, Y. Y.;Chen, J. C. and Lam, M. H. W., *Inorg. Chem.*, **2009**, *48*, 872-878.
20. Wang, P.;Leung, C. H.;Ma, D. L.;Lu, W. and Che, C. M., *Chemistry-an Asian Journal*, **2010**, *5*, 2271-2280.
21. Wang, P.;Leung, C. H.;Ma, D. L.;Sun, R. W. Y.;Yan, S. C.;Chen, Q. S. and Che, C. M., *Angew. Chem.-Int. Edit.*, **2011**, *50*, 2554-2558.
22. Miskowski, V. M. and Houlding, V. H., *Inorg. Chem.*, **1989**, *28*, 1529-1533.
23. Connick, W. B.;Henling, L. M.;Marsh, R. E. and Gray, H. B., *Inorg. Chem.*, **1996**, *35*, 6261-6265.
24. Paw, W.;Cummings, S. D.;Mansour, M. A.;Connick, W. B.;Geiger, D. K. and Eisenberg, R., *Coord. Chem. Rev.*, **1998**, *171*, 125-150.
25. Ni, J.;Zhang, X.;Wu, Y.-H.;Zhang, L.-Y. and Chen, Z.-N., *Chemistry – A European Journal*, **2011**, *17*, 1171-1183.
26. Hissler, M.;Connick, W. B.;Geiger, D. K.;McGarrah, J. E.;Lipa, D.;Lachicotte, R. J. and Eisenberg, R., *Inorg. Chem.*, **2000**, *39*, 447-457.

27.   Connick, W. B.;Miskowski, V. M.;Houlding, V. H. and Gray, H. B., *Inorg. Chem.*, **2000**, *39*, 2585-2592.

28.   Liu, Q. D.;Jia, W. L. and Wang, S. N., *Inorg. Chem.*, **2005**, *44*, 1332-1343.

29.   Pomestchenko, I. E.;Luman, C. R.;Hissler, M.;Ziessel, R. and Castellano, F. N., *Inorg. Chem.*, **2003**, *42*, 1394-1396.

30.   Nishida, J.;Maruyama, A.;Iwata, T. and Yamashita, Y., *Chem. Lett.*, **2005**, *34*, 592-593.

31.   Kato, M.;Shishido, Y.;Ishida, Y. and Kishi, S., *Chem. Lett.*, **2008**, *37*, 16-17.

32.   Kwok, E. C. H.;Chan, M. Y.;Wong, K. M. C.;Lam, W. H. and Yam, V. W. W., *Chem.-Eur. J.*, **2010**, *16*, 12244-12254.

33.   Bailey, J. A.;Hill, M. G.;Marsh, R. E.;Miskowski, V. M.;Schaefer, W. P. and Gray, H. B., *Inorg. Chem.*, **1995**, *34*, 4591-4599.

34.   Lai, S. W.;Chan, M. C. W.;Cheung, K. K. and Che, C. M., *Inorg. Chem.*, **1999**, *38*, 4262-4267.

35.   Yam, V. W. W.;Wong, K. M. C. and Zhu, N. Y., *Journal of the American Chemical Society*, **2002**, *124*, 6506-6507.

36.   Yam, V. W. W.;Chan, K. H. Y.;Wong, K. M. C. and Zhu, N. Y., *Chem.-Eur. J.*, **2005**, *11*, 4535-4543.

37.   Wong, K. M. C. and Yam, V. W. W., *Coord. Chem. Rev.*, **2007**, *251*, 2477-2488.

38.   Tam, A. Y. Y.;Wong, K. M. C.;Wang, G. X. and Yam, V. W. W., *Chem. Commun.*, **2007**, 2028-2030.

39.   Tong, G. S. M.;Law, Y. C.;Kui, S. C. F.;Zhu, N. Y.;Leung, K. H.;Phillips, D. L. and Che, C. M., *Chem.-Eur. J.*, **2010**, *16*, 6540-6554.

40.   Chan, K. H. Y.;Chow, H. S.;Wong, K. M. C.;Yeung, M. C. L. and Yam, V. W. W., *Chem. Sci.*, **2010**, *1*, 477-482.

41.   Garner, K. L.;Parkes, L. F.;Piper, J. D. and Williams, J. A. G., *Inorg. Chem.*, **2010**, *49*, 476-487.

42.   Lai, S. W.;Chan, M. C. W.;Cheung, T. C.;Peng, S. M. and Che, C. M., *Inorg. Chem.*, **1999**, *38*, 4046-4055.

43.   Fornies, J.;Fuertes, S.;Lopez, J. A.;Martin, A. and Sicilia, V., *Inorg. Chem.*, **2008**, *47*, 7166-7176.

44.   Diez, A.;Fornies, J.;Fuertes, S.;Lalinde, E.;Larraz, C.;Lopez, J. A.;Martin, A.;Moreno, M. T. and Sicilia, V., *Organometallics*, **2009**, *28*, 1705-1718.

45.   Fornies, J.;Sicilia, V.;Larraz, C.;Camerano, J. A.;Martin, A.;Casas, J. M. and Tsipis, A. C., *Organometallics*, **2010**, *29*, 1396-1405.

46.   Cave, G. W. V.;Alcock, N. W. and Rourke, J. P., *Organometallics*, **1999**, *18*, 1801-1803.

47.   Cave, G. W. V.;Fanizzi, F. P.;Deeth, R. J.;Errington, W. and Rourke, J. P., *Organometallics*, **2000**, *19*, 1355-1364.

48.   Berenguer, J. R.;Lalinde, E. and Torroba, J., *Inorg. Chem.*, **2007**, *46*, 9919-9930.

49.   Lu, W.;Chan, M. C. W.;Cheung, K. K. and Che, C. M., *Organometallics*, **2001**, *20*, 2477-2486.

50.   Kui, S. C. F.;Chui, S. S. Y.;Che, C. M. and Zhu, N. Y., *Journal of the American Chemical Society*, **2006**, *128*, 8297-8309.

51.   Kulikova, M. V.;Balashev, K. P. and Erzin, K., *Russian Journal of General Chemistry*, **2003**, *73*, 1839-1845.

52.   Cheung, T. C.;Cheung, K. K.;Peng, S. M. and Che, C. M., *J. Chem. Soc.-Dalton Trans.*, **1996**, 1645-1651.

53.   Song, D. T.;Wu, Q. G.;Hook, A.;Kozin, I. and Wang, S. N., *Organometallics*, **2001**, *20*, 4683-4689.

54. Lai, S. W.;Lam, H. W.;Lu, W.;Cheung, K. K. and Che, C. M., *Organometallics*, **2002**, *21*, 226-234.

55. Liu, Q. D.;Thorne, L.;Kozin, I.;Song, D. T.;Seward, C.;D'Iorio, M.;Tao, Y. and Wang, S. N., *J. Chem. Soc.-Dalton Trans.*, **2002**, 3234-3240.

56. Lu, W.;Mi, B. X.;Chan, M. C. W.;Hui, Z.;Che, C. M.;Zhu, N. Y. and Lee, S. T., *Journal of the American Chemical Society*, **2004**, *126*, 4958-4971.

57. Wang, Z. X.;Turner, E.;Mahoney, V.;Madakuni, S.;Groy, T. and Li, J. A., *Inorg. Chem.*, **2010**, *49*, 11276-11286.

58. Che, C. M.;Fu, W. F.;Lai, S. W.;Hou, Y. J. and Liu, Y. L., *Chem. Commun.*, **2003**, 118-119.

59. Williams, J. A. G.;Beeby, A.;Davies, E. S.;Weinstein, J. A. and Wilson, C., *Inorg. Chem.*, **2003**, *42*, 8609-8611.

60. Kanbara, T.;Okada, K.;Yamamoto, T.;Ogawa, H. and Inoue, T., *Journal of Organometallic Chemistry*, **2004**, *689*, 1860-1864.

61. Kui, S. C. F.;Sham, I. H. T.;Cheung, C. C. C.;Ma, C. W.;Yan, B. P.;Zhu, N. Y.;Che, C. M. and Fu, W. F., *Chem.-Eur. J.*, **2007**, *13*, 417-435.

62. Koo, C. K.;Ho, Y. M.;Chow, C. F.;Lam, M. H. W.;Lau, T. C. and Wong, W. Y., *Inorg. Chem.*, **2007**, *46*, 3603-3612.

63. Lee, C. S.;Sabiah, S.;Wang, J. C.;Hwang, W. S. and Lin, I. J. B., *Organometallics*, **2010**, *29*, 286-289.

64. Liu, R.;Li, Y. J.;Li, Y. H.;Zhu, H. J. and Sun, W. F., *J. Phys. Chem. A*, **2010**, *114*, 12639-12645.

65. Ma, B.;Djurovich, P. I.;Yousufuddin, M.;Bau, R. and Thompson, M. E., *Journal of Physical Chemistry C*, **2008**, *112*, 8022-8031.

66. Tong, G. S. M. and Che, C. M., *Chem.-Eur. J.*, **2009**, *15*, 7225-7237.

67. Cornioley-Deuschel, C.;Ward, T. and Von Zelewsky, A., *Helvetica Chimica Acta*, **1988**, *71*, 130-133.

68. Diez, A.;Fornies, J.;Larraz, C.;Lalinde, E.;Lopez, J. A.;Martin, A.;Moreno, M. T. and Sicilia, V., *Inorg. Chem.*, **2010**, *49*, 3239-3251.

69. Tam, A. Y. Y.;Lam, W. H.;Wong, K. M. C.;Zhu, N. Y. and Yam, V. W. W., *Chem.-Eur. J.*, **2008**, *14*, 4562-4576.

70. Lehn, J., *Angewandte Chemie. International edition in English*, **1990**, *29*, 1304-1319.

71. Hunter, C. A., *Chemical Society Reviews*, **1994**, *23*, 101-109.

72. Swiegers, G. F. and Malefetse, T. J., *Chem. Rev.*, **2000**, *100*, 3483-3537.

73. Turner, D. R.;Pastor, A.;Alajarin, M. and Steed, J. W., in *Supramolecular Assembly Via Hydrogen Bonds I*, Springer-Verlag Berlin, Berlin, 2004, vol. 108, pp. 97-168.

74. Jeffrey, G. A. and Saenger, W., *HYDROGEN BONDING IN BIOLOGICAL STRUCTURES*, 1991.

75. Desiraju, G. R. and Steiner, T., *The weak Hydrogen Bond in Structural Chemistry and Biology*, Oxford University Press, 1999.

76. Steiner, T., *Angew. Chem.-Int. Edit.*, **2002**, *41*, 48-76.

77. Ruben, M.;Rojo, J.;Romero-Salguero, F. J.;Uppadine, L. H. and Lehn, J. M., *Angewandte Chemie International Edition*, **2004**, *43*, 3644-3662.

78. Fujita, M.;Tominaga, M.;Hori, A. and Therrien, B., *Accounts Chem. Res.*, **2005**, *38*, 369-378.

79. Puddephatt, R. J., *Coord. Chem. Rev.*, **2001**, *216*, 313-332.

80. Zangrando, E.;Casanova, M. and Alessio, E., *Chem. Rev.*, **2008**, *108*, 4979-5013.

81. Burrows, A. D.;Chan, C. W.;Chowdhry, M. M.;McGrady, J. E. and Mingos, D. M. P., *Chemical Society Reviews*, **1995**, *24*, 329-&.

82. Braga, D. and Grepioni, F., *Coord. Chem. Rev.*, **1999**, *183*, 19-41.

83. Yuen, M. Y.;Roy, V. A. L.;Lu, W.;Kui, S. C. F.;Tong, G. S. M.;So, M. H.;Chui, S. S. Y.;Muccini, M.;Ning, J. Q.;Xu, S. J. and Che, C. M., *Angew. Chem.-Int. Edit.*, **2008**, *47*, 9895-9899.
84. Yip, J. H. K. and Vittal, J. J., *Inorg. Chem.*, **2000**, *39*, 3537-3543.
85. Takahashi, O.;Kohno, Y. and Nishio, M., *Chem. Rev.*, **2010**, *110*, 6049-6076.
86. Nishio, M., *Crystengcomm*, **2004**, *6*, 130-158.
87. Nishio, M.;Umezawa, Y.;Honda, K.;Tsuboyama, S. and Suezawa, H., *Crystengcomm*, **2009**, *11*, 1757-1788.
88. Constable, E. C.;Housecroft, C. E.;Kopecky, P.;Schonhofer, E. and Zampese, J. A., *Crystengcomm*, **2011**, *13*, 2742-2752.
89. Steiner, T., *Chem. Commun.*, **1997**, 727-734.
90. Desiraju, G. R., *Accounts Chem. Res.*, **2002**, *35*, 565-573.
91. Lee, C. H.;Su, F. Y.;Lin, Y. H.;Chou, C. H. and Lee, K. M., *Crystengcomm*, **2011**, *13*, 2318-2323.
92. Maly, K. E.;Maris, T.;Gagnon, E. and Wuest, J. D., *Cryst. Growth Des.*, **2006**, *6*, 461-466.
93. Stephenson, M. D. and Hardie, M. J., *Cryst. Growth Des.*, **2006**, *6*, 423-432.
94. Casas, J. M.;Diosdado, B. E.;Falvello, L. R.;Fornies, J. and Martin, A., *Inorg. Chem.*, **2005**, *44*, 9444-9452.
95. Brammer, L.;Charnock, J. M.;Goggin, P. L.;Goodfellow, R. J.;Orpen, A. G. and Koetzle, T. F., *J. Chem. Soc.-Dalton Trans.*, **1991**, 1789-1798.
96. Casas, J. M.;Falvello, L. R.;Fornies, J.;Martin, A. and Welch, A. J., *Inorg. Chem.*, **1996**, *35*, 6009-6014.
97. Chatterjee, S.;Krause, J. A.;Oliver, A. G. and Connick, W. B., *Inorg. Chem.*, **2010**, *49*, 9798-9808.
98. Wehman-Ooyevaar, I. C. M.;Grove, D. M.;Kooijman, H.;Van der Sluis, P.;Spek, A. L. and Van Koten, G., *Journal of the American Chemical Society*, **1992**, *114*, 9916-9924.
99. Steiner, T. and Koellner, G., *J. Mol. Biol.*, **2001**, *305*, 535-557.
100. Braga, D.;Grepioni, F. and Tedesco, E., *Organometallics*, **1998**, *17*, 2669-2672.
101. Malone, J. F.;Murray, C. M.;Charlton, M. H.;Docherty, R. and Lavery, A. J., *J. Chem. Soc.-Faraday Trans.*, **1997**, *93*, 3429-3436.
102. Hunter, C. A.;Meah, M. N. and Sanders, J. K. M., *Journal of the American Chemical Society*, **1990**, *112*, 5773-5780.
103. Yamauchi, Y.;Yoshizawa, M. and Fujita, M., *Journal of the American Chemical Society*, **2008**, *130*, 5832-+.
104. Bruning, W.;Freisinger, E.;Sabat, M.;Sigel, R. K. O. and Lippert, B., *Chem.-Eur. J.*, **2002**, *8*, 4681-4692.
105. Qin, Z. Q.;Jennings, M. C. and Puddephatt, R. J., *Chem. Commun.*, **2001**, 2676-2677.
106. Qin, Z. Q.;Jennings, M. C. and Puddephatt, R. J., *Inorg. Chem.*, **2003**, *42*, 1956-1965.
107. Fleeman, W. L. and Connick, W. B., *Comments on Inorganic Chemistry*, **2002**, *23*, 205-230.
108. Siemeling, U.;Bausch, K.;Fink, H.;Bruhn, C.;Baldus, M.;Angerstein, B.;Plessow, R. and Brockhinke, A., *Dalton Transactions*, **2005**, 2365-2374.
109. Zhou, G. J.;Wang, Q.;Wang, X. Z.;Ho, C. L.;Wong, W. Y.;Ma, D. G.;Wang, L. X. and Lin, Z. Y., *J. Mater. Chem.*, **2010**, *20*, 7472-7484.
110. D'Andrade, B. W. and Forrest, S. R., *Adv. Mater.*, **2004**, *16*, 1585-1595.